Supplementary Information for

Site Specific NMR Characterization of Abeta-40 Oligomers Cross Seeded by Abeta-42 Oligomers

Han-Wen Chang,[a] Ho-I Ma,[a] Yi-Shan Wu,[a] Ming-Che Lee,[a] Eric Chung-Yueh Yuan,[a] Yu-Sheng Cheng,[a] Shing-Jong Huang,[b] Meng-Hsin Wu,[c] Ling-Hsien Tu,[c] Jerry Chun Chung Chan,[a*]

[a] Department of Chemistry, National Taiwan University, No. 1, Section 4, Roosevelt Road, Taipei, 10617, Taiwan.

[b] Instrumentation Center, National Taiwan University, No. 1, Section 4, Roosevelt Road, Taipei, 10617, Taiwan.

[c] Department of Chemistry, National Taiwan Normal University, No. 88, Section 4, Ting-Chow Road, Taipei, 11677, Taiwan.

* To whom correspondence should be addressed
E-mail: chanjcc@ntu.edu.tw

Table of Contents

MATERIALS AND METHODS 3
DISCUSSION 8
FIGURES 9
TABLES 43
REFERENCES 47

Materials and Methods

Bacterial Expression of β-Amyloid Peptides in Natural Abundance. The $A\beta_{40}$ peptide was expressed with a hexahistidine-tagged ubiquitin and a recognition site for TEV protease in the N-terminal. The plasmid of the fusion protein was transformed to *Escherichia coli* BL21 competent cell. A single colony was picked and grown in 50 mL of lysogeny broth (LB) medium containing Kanamycin (25 μg/mL) at 37 ℃ with orbital shaking at 140 rpm overnight. A 15 mL fraction of the culture was transferred to 1 L of LB medium, and the protein expression was induced at the OD_{600} value of 0.8–1.0 with isopropyl β-D-1-thiogalactopyranoside (IPTG, 1 mM). Cells were harvested at 8 000 *g* (4 ℃) after 8 h of incubation (37 ℃, 140 rpm). The pellet was resuspended in 30 mL of lysis buffer (20 mM Tris, 150 mM NaCl, pH 8.0). The cells were sonicated in an ice bath and centrifuged (10 000 *g*, 1.5 h) to pellet the inclusion bodies. After discarding the supernatant, the inclusion bodies were dispersed in solubilization buffer (20 mM Tris, 150 mM NaCl, 2 M urea, pH 10.0) overnight. After removing the undissolved pellet by centrifugation, the supernatant was loaded into a nickel-nitriloacetic acid (Ni–NTA) column (Histrap HP, 5 mL, GE Healthcare). The column was washed with buffer A (20 mM Tris, 150 mM NaCl, 5 M urea, pH 8.0) and buffer B (20 mM Tris, 150 mM NaCl, 5 M urea, 500 mM imidazole, pH 8.0) by applying a linear gradient from 2% to 100% of buffer B. The bounded Aβ fusion protein collected at ~30% was subsequently concentrated with Amicon Ultra-15 centrifugal filter unit (10 kDa MWCO) to 1 mL. The fusion protein was diluted five times with lysis buffer during TEV cleavage at 25 ℃ for 16 h. The solution was purified again with Ni–NTA column. The cleaved Aβ collected in the flow-through was concentrated with Amicon Ultra-15 centrifugal filter unit (3 kDa MWCO) to 5 mL and then injected into a Vydac C8 reverse-phase column of preparative scale for HPLC purification, utilizing a binary solvent gradient formed by solvent A (0.1 % trifluoroacetic acid in H_2O) and solvent B (95% acetonitrile, 4.9% H_2O, and 0.1% trifluoroacetic acid). Fractions containing the target product were collected at 37% of solvent B and lyophilized. The $A\beta_{42}$ peptide was similarly expressed as described for $A\beta_{40}$, except that 4 M of urea was used to prepare the solubilization buffer. The cleaved $A\beta_{42}$ collected in the flow-through was concentrated with Amicon Ultra-15 centrifugal filter unit (3 kDa MWCO) to 5 mL and then injected into an Agilent Zorbax 300SB-C8 reverse-phase column of preparative scale at 80 °C for HPLC purification. Fractions containing the target product were collected at 39% of solvent B and then lyophilized.

Preparation of ^{13}C enriched β-Amyloid Peptides. Isotopically enriched (^{13}C and ^{15}N) amino acids with 9-fluorenylmethoxycarbonyl (Fmoc) protection were obtained from CortecNet (Tilleuls, France) and Sigma-Aldrich (St. Louis, MO, USA). Unlabeled Fmoc-amino acids were obtained from ChinaPeptides (Wujiang, China). Peptides of unlabeled or site-specific labeled $A\beta_{40}$, with the sequence DAEFRHDSGYEVHHQKLVFFAEDVGSNKGAIIGLMVGGVV, were synthesized on a Liberty Lite microwave peptide synthesizer (CEM Corp., Matthews, NC). A loading scale of Cl-MPA ProTide Resin (LL) at 0.16 mmol/g was used as solid support. Diisopropylcarbodiimide (DIC) was used to activate the carboxylic group of Fmoc-protected amino acid and 10% piperazine (w/v) in a solution of ethanol (EtOH) and N-methylpyrrolidone (NMP) (10:90) was used to remove the Fmoc group in each reaction cycle. The synthesis

scale was 0.05 mmol. A mixture of 3-fold excess isotopically labeled amino acids and 2-fold excess unlabeled amino acids was used for coupling of labeled residues and 5-fold excess unlabeled amino acids was used for other unlabeled residues. The coupling step was carried out for 5 min at 75 °C for all residues except Histidine which was double coupled for 12 min at 50 °C to minimize racemization. Arginine, Serine and Valine were all double coupled for 5 min at 75 °C to increase coupling efficiency. Crude peptides were cleaved from the resin using 92.5% trifluoroacetic acid (TFA) with 2.5% Triisopropylsilane (TIS), 2.5% deionized (DI) water, and 2.5% 2,2'-(Ethylenedioxy)diethanethiol (DODT) and then precipitated in cold diethyl ether. Peptides were collected by filtration and then lyophilized. Crude peptides were purified by reverse-phase high-performance liquid chromatography (HPLC) using a Vydac C18 preparative column and water/acetonitrile gradient consisting of 0.1% TFA as mobile phase. Samples of 5 mg per injection were first dissolved in 1 mL of TFA and then diluted to 5 mL with 30% acetonitrile in DI water before injecting. Fractions were collected, lyophilized, and subjected to mass spectrometry.

Preparation of $RM_{CO520}Aβ_{40}$. All chemicals were obtained from Acros Organics unless stated otherwise. Purified $Aβ_{40}$ peptides were dissolved in 1,1,1,3,3,3-hexafluoro-2-propanol (HFIP) at a concentration of 1 mM, sonicated in a bath-type sonicator for 1.5 h at 0 °C, dried with a gentle stream of nitrogen, and lyophilized overnight. The HFIP-pretreated peptide (ca. 1 mg) was dissolved in 0.2 mL of 50 mM NaOH(aq). After sonication for 5 min, the solution was diluted with 0.7 mL of deionized water and 0.1 mL of ammonium acetate buffer (1 M) and agitated by sonication for another 5 min. After centrifugation (200 000 *g*) at 4 °C for 1 h, the top 90% of the supernatant was collected and its concentration was determined by UV absorbance based on the extinction coefficient of 0.2956 $(mg/mL)^{-1}cm^{-1}$. The supernatant was diluted with ammonium acetate (100 mM) buffer to a peptide concentration of 100 μM and pH 7.4. To prepare the target reverse micelle solution, 0.5 g of Igepal CO520 (Sigma-Aldrich) was dissolved in 15 mL of cyclohexane, to which 0.5 mL of freshly prepared Aβ monomer solution (100 μM) was slowly added, resulting in the water loading ratio ($w_0 = n_{H_2O}/n_{CO520}$) equal to 24.5. The solution was incubated for 7 days under quiescent conditions at 25 °C. To back extract the Aβ peptides from the RM solution, the stripping buffer ($ZnCl_2$, 50 μM) was added to the RM solution with a volume ratio of 1:1, followed by centrifugation (12 000 *g*, 15 min). After removing the top layer of cyclohexane, the sample was lyophilized. The dried sample was washed by cold *tert*-butyl methyl ether to remove CO520. The residual ether was removed by drying *in vacuo* and then stored at –20 °C. A typical yield of the lyophilized product was 0.575 mg. The sample of $RM_{CO520}Aβ_{42}$ was prepared similarly.

Preparation of $RM_{CO520}Aβ_{42/40}$. The $RM_{CO520}Aβ_{42}$ solution containing 0.25 mL of $Aβ_{42}$ monomers (100 μM in NH_4Ac) and 0.25 g of CO520 in 7.5 mL of cyclohexane was incubated for 3 days under quiescent conditions at 25 °C. After that, 3.875 mL of CO520 in cyclohexane was added to the solution, followed by the addition of freshly prepared $Aβ_{40}$ monomer (0.125 mL, 100 μM). After further incubating for 3 days, another batch of 3.875 mL of CO520 in cyclohexane and 0.125 mL of $Aβ_{40}$ monomer solution were added.

The resultant mixture was incubated for another 4 days, followed by the procedure of back extraction as described above.

Preparation of $RM_{CO520}A\beta_{42/40}$ fibrils. The lyophilized samples of $RM_{CO520}A\beta_{42/40}$ after NMR measurements were resuspended in phosphate buffer (20 mM sodium phosphate, 200 μM EDTA, 0.02% NaN_3, pH 7.4) at a concentration of 1 mg/mL under150 rpm orbital shaking at 37 ℃ for 19 days. The fibril sample was collected by centrifugation and washed by DI water for three times. The wet pellet was transferred to an NMR rotor by centrifugation.

TMV particles. A volume of 500 μL of Tris buffer (10 mM, pH 7.4) was added to homogenize several pieces of TMV-infected tobacco leaf (9 mg) in an Eppendorf. The TMV solution was centrifuged at 12 000 *g* for 20 min at 4 ℃ to remove the debris. The supernatant was kept at −80 ℃ for subsequent use.

Elemental Analysis. The sample (3–4 mg) in tin capsule was weighed and loaded into the autosampler. The analysis was carried out with a vario EL cube NCSH elemental analyzer (Elementa, Germany), which was calibrated using sulfanilic acid as the standard. The error analysis using bootstrapping method was conducted with 1000 resampled data.[1] For each resampled data, %($A\beta_{40}$) and %(CO520) were estimated by minimizing χ using the minimize function in the scipy.optimize module (by the default BFGS method), [2,3] where the initial guesses were randomly chosen from 0−100%. The explicit expression of χ is given in the footnote of Table S1.

Scanning TEM (STEM). A volume of 10 μL of the sample was deposited onto 200-mesh Formvar carbon-coated copper grids (Ted Pella Inc., Redding, CA) for 2 min. The grid was washed by DI water twice, followed by the deposition of 5 μL of the TMV solution. The grid was washed with DI water again. After drying in a desiccator for 20 min, the grid was examined with a Hitachi SU8220 scanning transmission electron microscope operated at 20 kV. The procedure to estimate the MW of the oligomers is described as follows. Given that the width of rod-like TMV is 18 nm and that the mass-per-length of TMV is 131 kDa/nm, the mass-per-area of TMV is calculated as 7.3 kDa/nm^2. The image intensities of TMV were integrated over rectangular areas (22 × 18 nm^2) centered on TMV segments (I_{TMV}) and over equal areas of background in close proximity (B_{TMV}). The image intensities, viz. I_{olig} and B_{olig}, of $RM_{CO520}A\beta_{40}$ were obtained similarly by integrating over circular areas of 40 nm in diameter. The MW of $RM_{CO520}A\beta_{40}$ (MW_{app}) was calculated as $7.3 \times 22 \times 18 \times \left(\frac{I_{olig}-B_{olig}}{I_{TMV}-B_{TMV}}\right)$ in the unit of kDa. By removing the contribution from CO520, the MW of $A\beta_{40}O$ was estimated by $MW_{app} \times \frac{4330}{4330+441\times r}$, where r is the molar ratio of $A\beta_{40}$ to CO520 for $RM_{CO520}A\beta_{40}$.

Bright-Field TEM. The samples were deposited onto 200-mesh Formvar carbon-coated copper grids (Ted Pella Inc., Redding, CA) for 1 min. The grid was washed by DI water twice, then negatively stained with 2%

uranyl acetate for 1 min. After drying at room temperature, the grid was studied with a Hitachi H-7100 transmission electron microscope operated at 75 kV.

ThT Assay. The ThT assay was conducted with reference to the protocol published in the literature. [4] The pellet of $RM_{CO520}A\beta$ was resuspended in the monomer solution of $A\beta_{40}$ (25 μM) in phosphate buffer (20 mM sodium phosphate, 200 μM EDTA, 0.02% NaN_3, pH 7.4) to desired concentration. A stock solution of 1.2 mM Thioflavin T (ThT) was prepared by dissolving ThT in the phosphate buffer and filtered before use. After mixing 200 μL of the Aβ solution and 1 μL of the ThT stock solution, the solution mixture was then pipetted into a non-binding plate (384-well, Corning 3575), with 45 μL per well and triplicate repeats for each sample. The plate was then sealed with a plastic film. The fluorescence signal was collected at 490 nm by a microplate reader (SpectraMax® i3x, Molecular Devices) with an excitation at 442 nm. The data were obtained every 5 minutes at 37 °C with continuous shaking between measurements. By the procedure of keep-one-discard-four, the total data points were reduced to one-fifth of the original size.

Dot Blot Assay. An aliquot of the sample (2.0 μL) was applied to a nitrocellulose membrane (Pall) of 0.22 μm pore size. The membrane was immersed in 15 mL of blocking buffer which contained 1% casein in phosphate-buffered saline with 0.1% Tween 20 (PBS-T). After incubating for 30 min in an orbital shaker, the membrane was transferred to a plastic bag, to which 1.0 mL of the antibody, either the 6E10 (mouse IgG1, Covance) or OMAB (mouse IgM, Agrisera), diluted with blocking buffer (1:1000 v/v), was added. After sealing the bag, the sample was incubated in a rocker for 2 h. The membrane was taken out and washed three times with PBS-T, agitating gently for 10 min in each wash. The membrane was then transferred to 15 mL of a solution of secondary antibody for which the goat anti-mouse IgG or IgM Alexa Fluor 790 (Jackson) was used. After incubating in the dark for 45 min, the membrane was washed three times with PBS-T as described above, followed by washing with DI water. The fluorescence signal of the membrane was examined with LI-COR Odyssey CLx Infrared Imaging System at a wavelength of 800 nm.

Dynamic Light Scattering. The size distribution of $RM_{CO520}A\beta$ was determined by dynamic light scattering (DLS) using a commercial instrument (Malvern Zetasizer ZS300).

Solid-State NMR. Unless stated otherwise, all NMR experiments were carried out at ^{13}C and ^{1}H frequencies of 100.63 and 400.13 MHz, respectively, on a Bruker Avance III spectrometer equipped with a 2.5 mm probe. The sample temperature was maintained at 281 K. For the ^{13}C–^{13}C dipolar-assisted rotational resonance (DARR) correlation spectroscopy,[5,6] the initial ^{13}C magnetization was prepared by $^{13}C\{^{1}H\}$ cross polarization with a contact time of 1.6 ms, where the ^{1}H nutation frequency was 70 kHz and that of ^{13}C was ramped and optimized with respect to the Hartmann-Hahn matching condition. During the mixing period of 200 ms, the ^{1}H nutation frequency was set to the spinning frequency. The durations of all ^{1}H and ^{13}C $\pi/2$ pulses were set to be 5 μs. The DARR spectra of the samples were measured at a spinning frequency of 20 kHz. Two pulse phase modulation proton decoupling of 80 kHz was applied during both the t_1 evolution and acquisition

periods.[7] The recycle delay was 2 s. A total of 128 increments were acquired at steps of 40 μs. The number of transients accumulated for each t_1 increment was 128. TPPM decoupling of 100 kHz was set during t_1 and t_2 evolution periods, and the same strength was applied during the mixing time. An exponential window function (EM) with 1.5 ppm line broadening and a 90° shifted squared sine bell window function (QSINE, SSB = 2) were applied in the t_2 and t_1 dimensions before the Fourier transformations. ^{13}C chemical shifts were externally referenced to neat tetramethylsilane (TMS) using adamantane as the secondary reference (the more deshielded peak assigned to 38.48 ppm).[8] For the TALOS-N calculations, all chemical shifts were referenced to sodium trimethylsilylpropanesulfonate (DSS) by adding the neat-TMS referenced chemical shifts by 2.01 ppm.[8]

Discussion

Encapsulation of Aβ peptides within Reverse Micelles. The extracellular Aβ taken up by murine cortical neurons and neuroblastoma can be trafficked into vesicular compartments and thereby aggregates to form high-MW species.[9] The significance of extracellular vesicles has also been observed in tau pathology.[10] Previously, we attempted to incubate $A\beta_{40}$ peptides in liposomes, where the primary nucleation was the major early event.[11,12] This approach is partly based on the notion that non-ionic phospholipids can induce Aβ aggregation.[13] Although it is possible to use liposomes to exert some level of control over the aggregation pathway of $A\beta_{40}$ peptides, the structural integrity of liposomes were compromised by the $A\beta_{40}$ peptides localized on the inner or outer surface of the lipid bilayers. To completely suppress the nucleation pathways of fibril fragmentation and fibril-assisted nucleation, Aβ peptides have to be incubated in a confined space. As a proof of concept, we used the RMs formed by sodium bis(2-ethylhexyl) sulfosuccinate (AOT)/isooctane/Tris buffer to prepare the aggregates of $A\beta_{40}$ ($RM_{AOT}A\beta_{40}$), for which a series of techniques including DLS, ThT fluorescence assay, the dot-blot assay with the oligomer-specific monoclonal antibody, immunogold staining, and analytical SEC were used to validate that $RM_{AOT}A\beta_{40}$ are oligomeric aggregates of $A\beta_{40}$.[14] However, the molar ratio of AOT:$A\beta_{40}$ in $RM_{AOT}A\beta_{40}$ was up to a factor of 408 even after sample washing, rendering any subsequent NMR and biochemical characterization of the oligomers very difficult. By contrast, there was a significant reduction of the surfactant amount in $RM_{CO520}A\beta$. We attributed this favorable property to the fact that the chemical moiety of the hydrophilic head of CO520 is very similar to that of polyethylene glycol, so that the non-ionic interaction between CO520 and Aβ peptides was smaller than that between AOT and Aβ, which is electrostatic in nature. Consequently, we do not expect a substantial modulation of the molecular structures of $A\beta_{40}$Os by the templating effect of the surfactants, if any. Thus, the nucleation process occurred within the RMs should be rather similar to the primary nucleation process in bulk solution. Our RM system comprised three chemical components, viz., apolar cyclohexane, aqueous buffered peptide solution, and the detergents constituting the surface between these phases. Because Aβ peptides are amphipathic, the possibility that the peptides get sequestered into the organic phase or the phase separation boundaries requires a careful consideration. At the first glance, in situ study by circular dichroism or solution-state NMR would be desired to verify whether the peptides are mainly distributed into the aqueous phase. However, the surfactant molecules CO520 have a strong absorption in the range of 220–280 nm. Measurements by solution-state NMR is also impractical because the effective peptide concentration, in the presence of the organic phase, was in the regime of 3 μM. Fortunately, infrared spectroscopy and molecular dynamics simulations have convincingly shown that $A\beta_{40}$ peptides preferentially reside in the aqueous phase of RMs.[15,16]

Figures

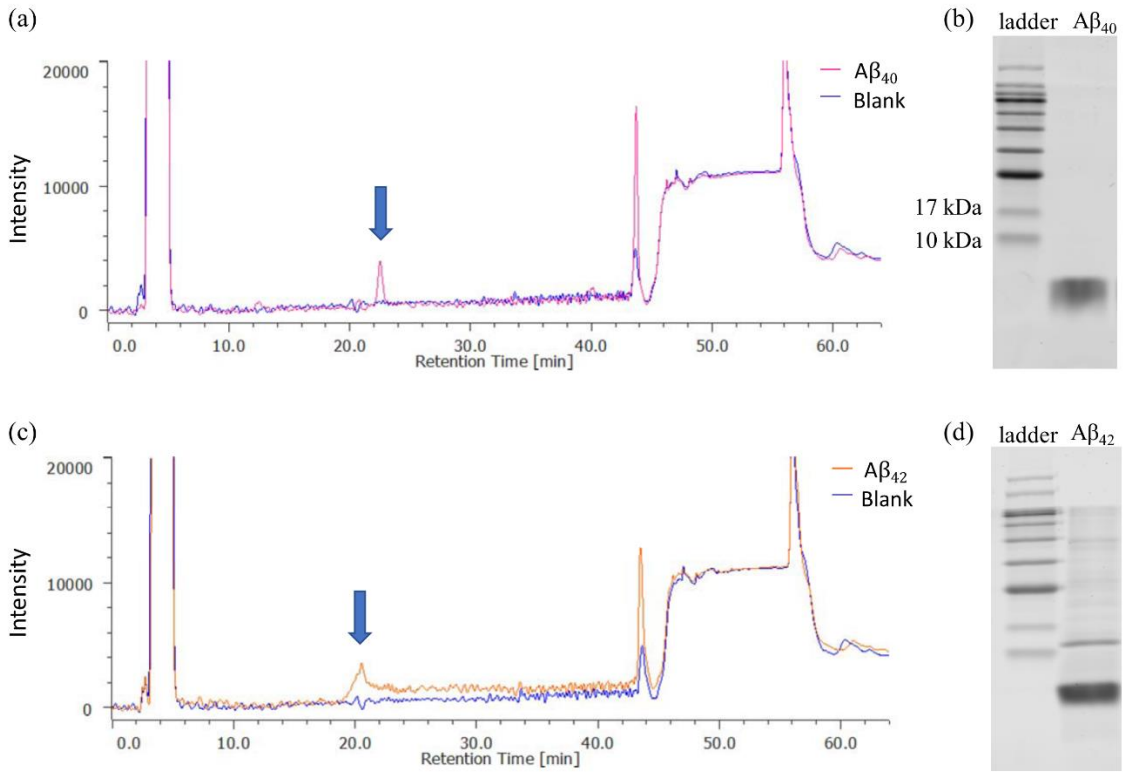

Fig. S1. Purification of Aβ peptides. (a) HPLC chromatogram of $A\beta_{40}$ peptides acquired by an analytical C18 column (SpectroChrom, SCpak ODS-P, 5 μm). The arrow indicates the retention time at which the sample was collected. (b) SDS-PAGE of the collected $A\beta_{40}$ peptides. (c, d) Results obtained for $A\beta_{42}$.

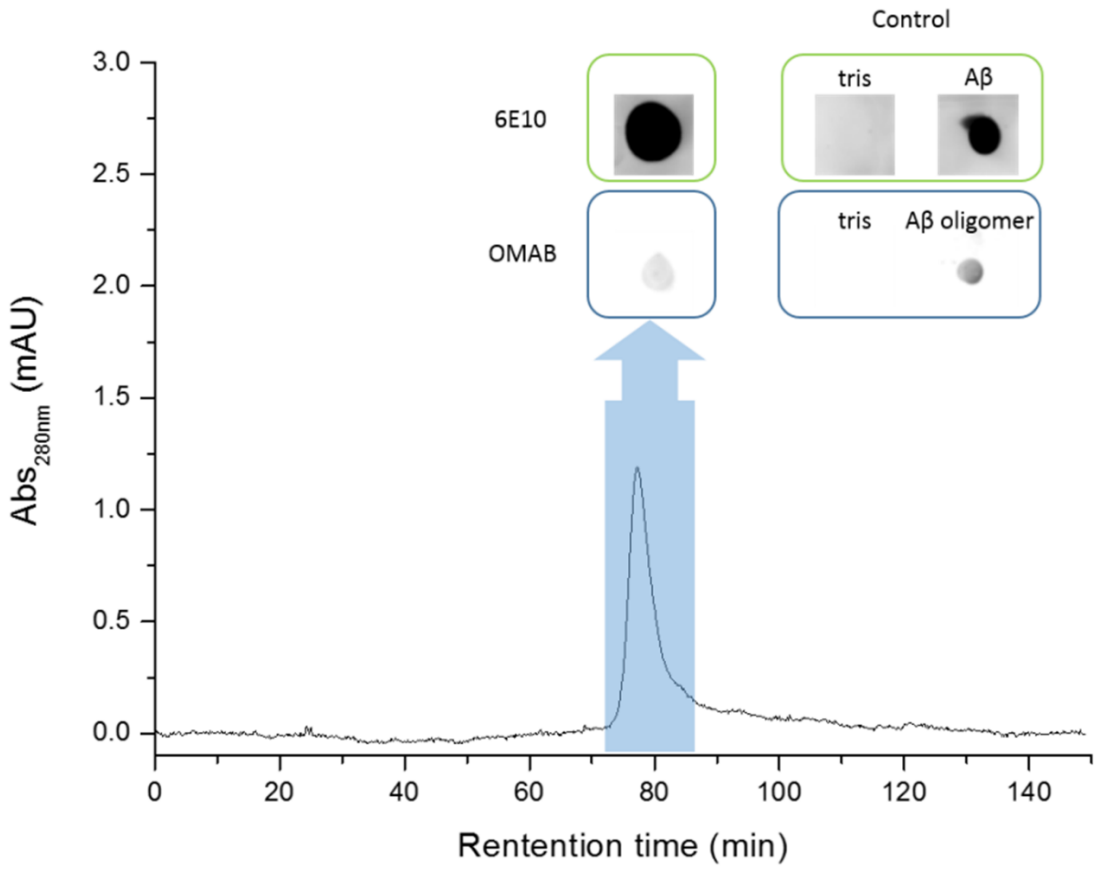

Fig. S2. Size exclusion chromatogram (SEC) profile of the freshly prepared $A\beta_{40}$ monomers using the column of GE Hiload (16/600 Superdex, 75 pg). The collected sample was tested by dot-blot assay using the antibodies of 6E10 and OMAB. Tris buffer, $A\beta_{40}$ peptides, and the $A\beta_{40}$ oligomers prepared at low temperature were used as the control samples. The results for 6E10 confirmed that the collected fraction contained Aβ peptides. The results for OMAB indicated that the peptides were mainly in monomeric state.

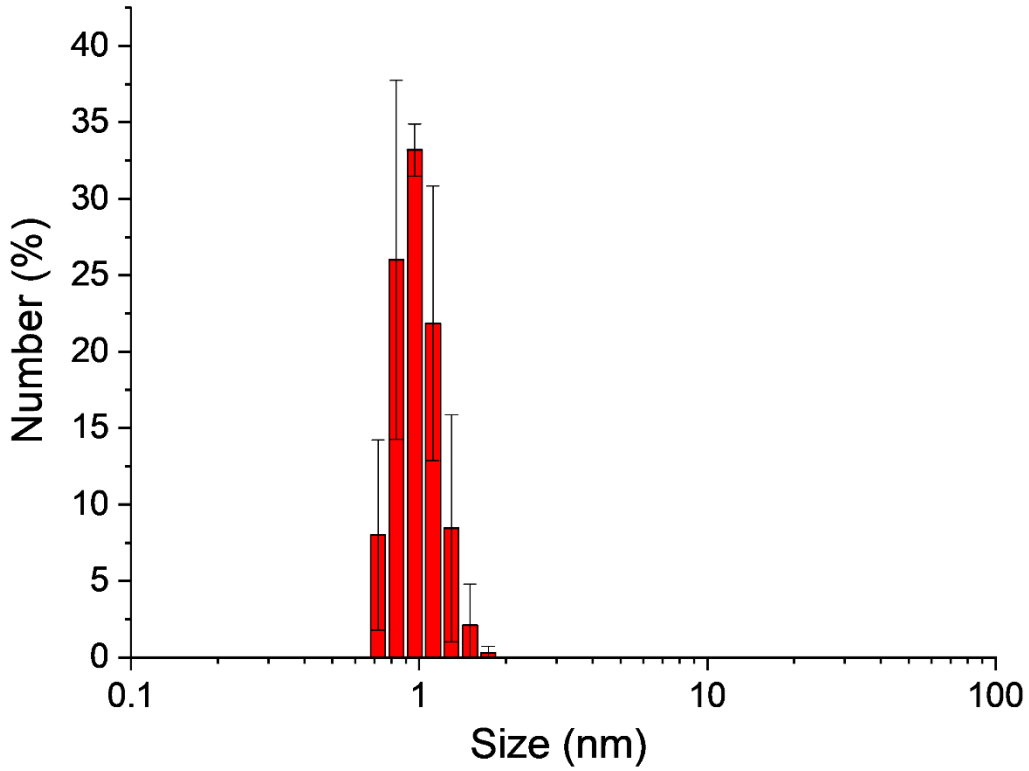

Fig. S3. DLS data of the freshly prepared $A\beta_{40}$ monomers. The results revealed that no sizable aggregates were present in the solution.

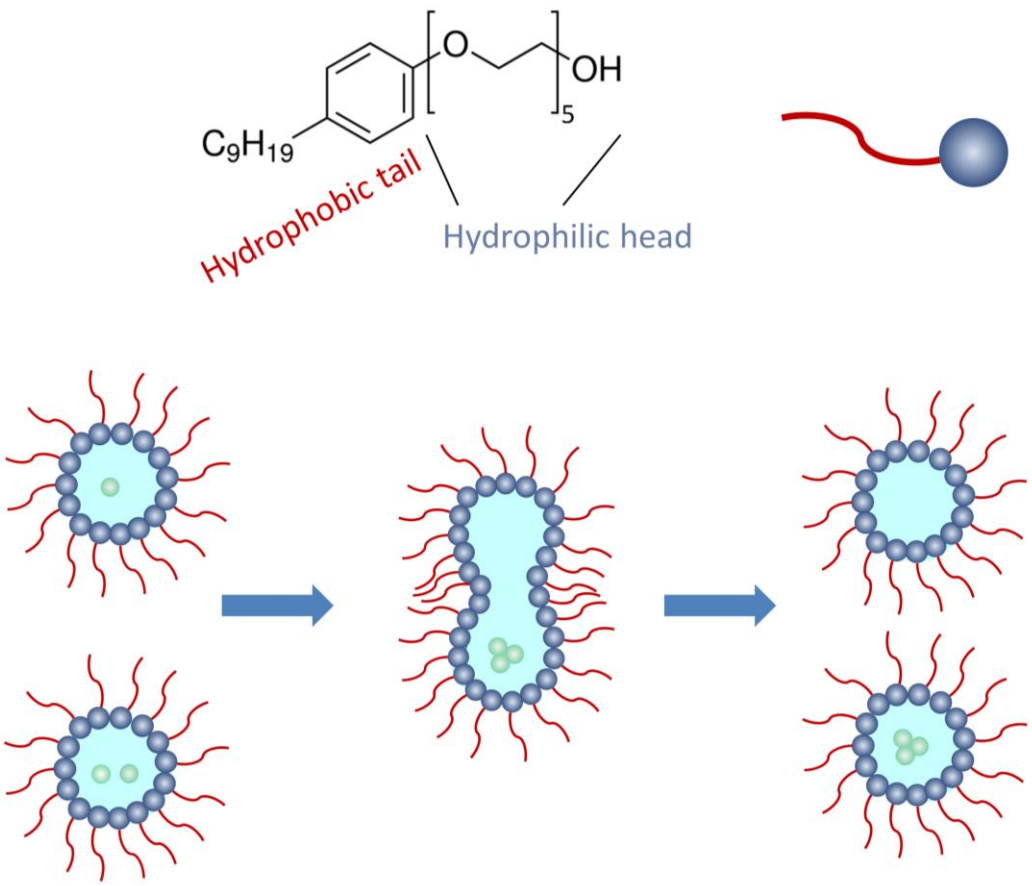

Fig. S4. Schematic illustration of the aggregation process of Aβ peptides upon the coalescence and separation of reverse micelles (RM) formed by the surfactants of CO520. The regions colored in cyan represent the water phase. The hydrophobic tails of the surfactants are in the oil phase (cyclohexane).

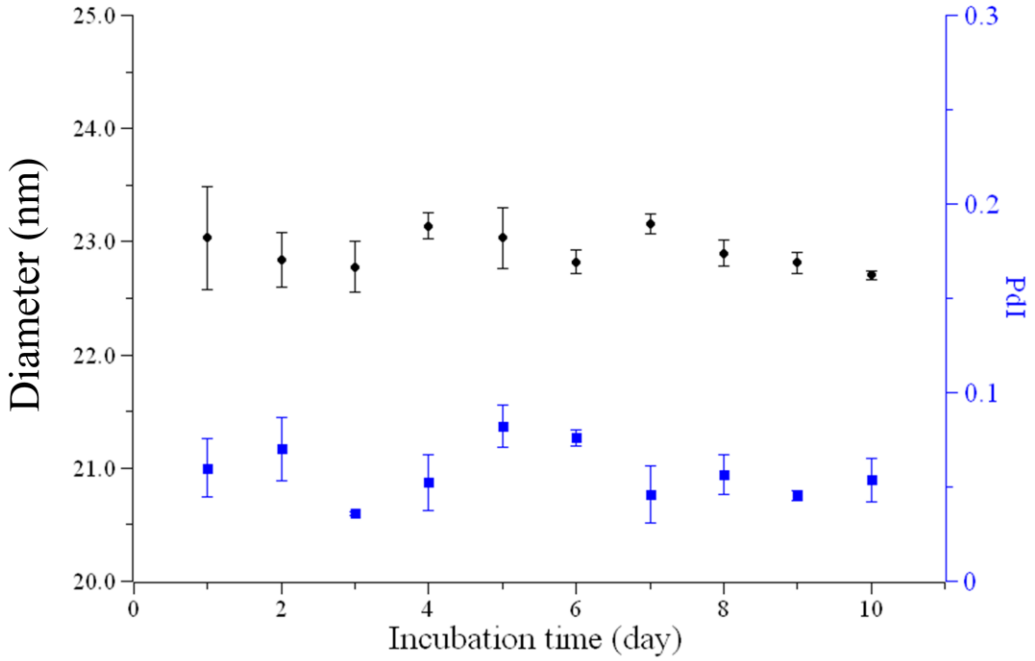

Fig. S5. Typical DLS data of Aβ peptides incubated in RMs. The average diameter of the RMs prepared in this batch was about 23 nm with excellent size homogeneity (PdI < 0.1).

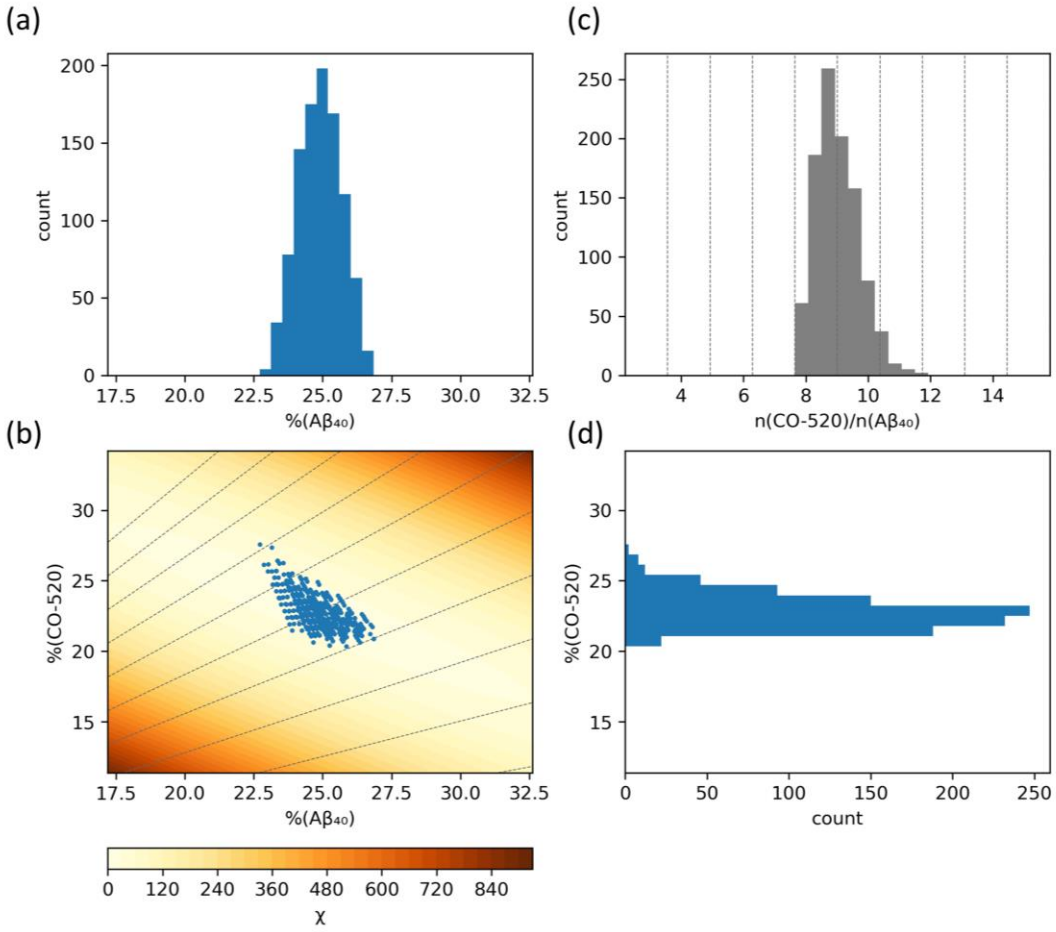

Fig. S6. Quantification of $A\beta_{40}$ and CO520 by EA experiments. Six independent EA data (two samples and triplicate measurements for each) were acquired and analyzed. The error analysis was conducted using bootstrapping method with 1000 resampled data, marked in blue dots and summarized in the histograms for the corresponding dimensions (a and d). The profile of the mean-square deviation between the calculated and experimental data (χ), as a function of the mass percentages of $A\beta_{40}$ and CO520 is depicted in (b). The molar ratio of CO520 and $A\beta_{40}$ was evaluated in (c). The mass percentages of CO520 and $A\beta_{40}$ were estimated to be 22.8% and 24.9%, respectively. The sum of their mass contributions was less than 100% because of the presence of other residual species such as $ZnCl_2$ in the samples. The molar ratio of CO520 and $A\beta_{40}$ was estimated to be 9.0 ± 0.7.

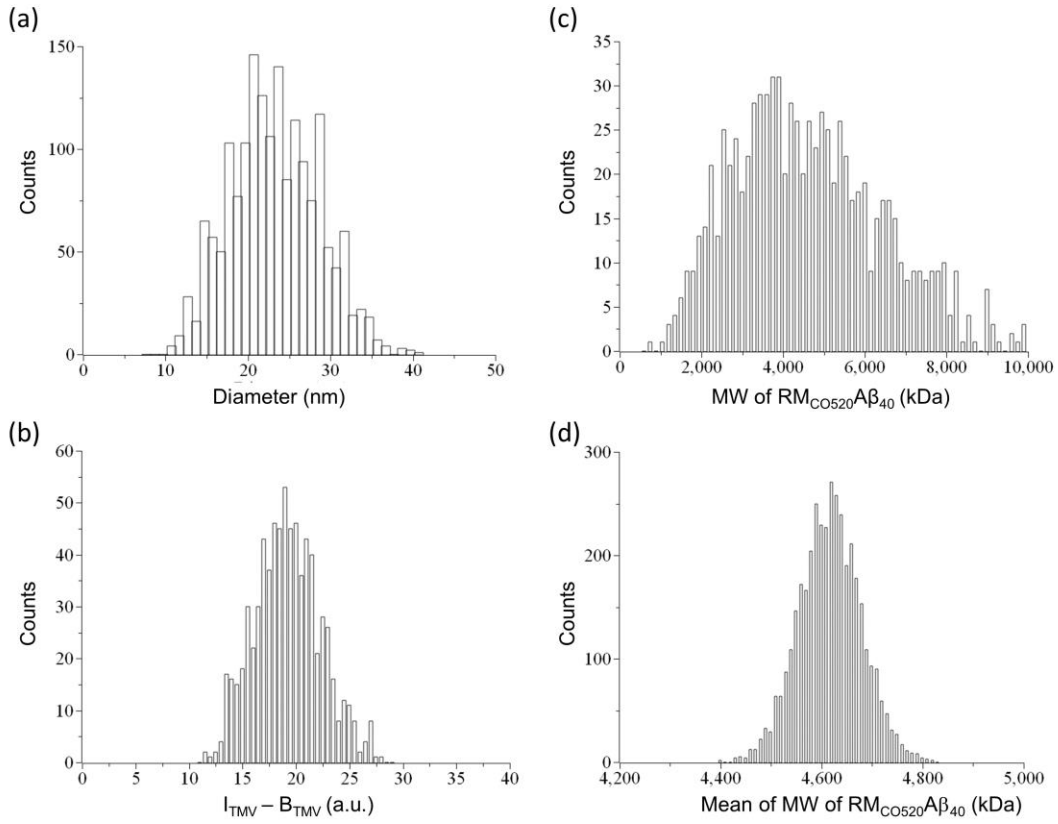

Fig. S7. (a) Size distribution of the spherical aggregates extracted from the STEM images of a mixture of RM$_{CO520}$Aβ$_{40}$ and TMV. A statistical analysis of the data comprising 1745 particles gave an average size of 23.1 ± 5.3 nm. **(b)** Intensity distribution of TMV, where I_{TMV} and B_{TMV} denote the intensity integrated over the same area centered on TMV segments and background in close proximity, respectively. The histogram plot shows the results of a total of 737 boxes. **(c)** MW distribution of RM$_{CO520}$Aβ$_{40}$ estimated with reference to the averaged (I_{TMV} – B_{TMV}). A total of 849 data points had been considered. **(d)** Distribution of 10,000 mean values calculated from the data in (c) by the bootstrapping resampling method. The mean of the MW of RM$_{CO520}$Aβ$_{40}$ was estimated to be 4617 kDa with a standard deviation of 1820 kDa.

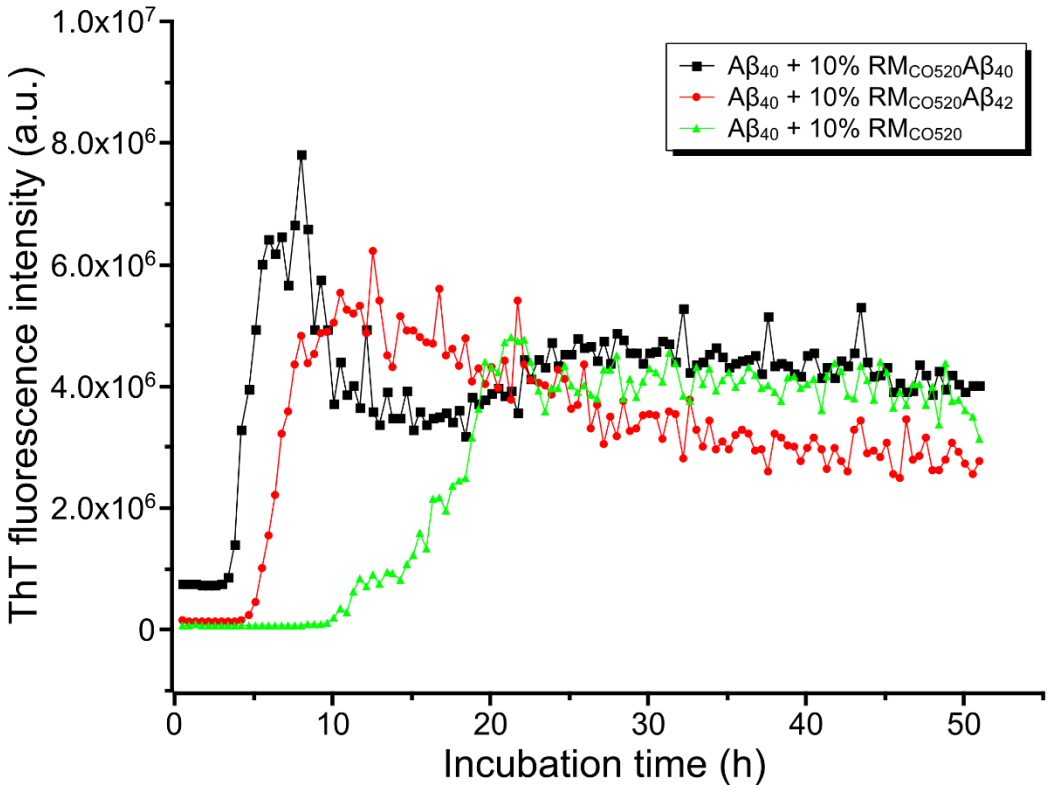

Fig. S8. ThT Fluorescence results for probing the seeding effects of $RM_{CO520}A\beta$. For all the measurements, the concentration of $A\beta_{40}$ monomer was 25 μM. The amount of the seeds was adjusted to 10 mole % of the monomers. RM_{CO520} was prepared in the absence of Aβ peptides.

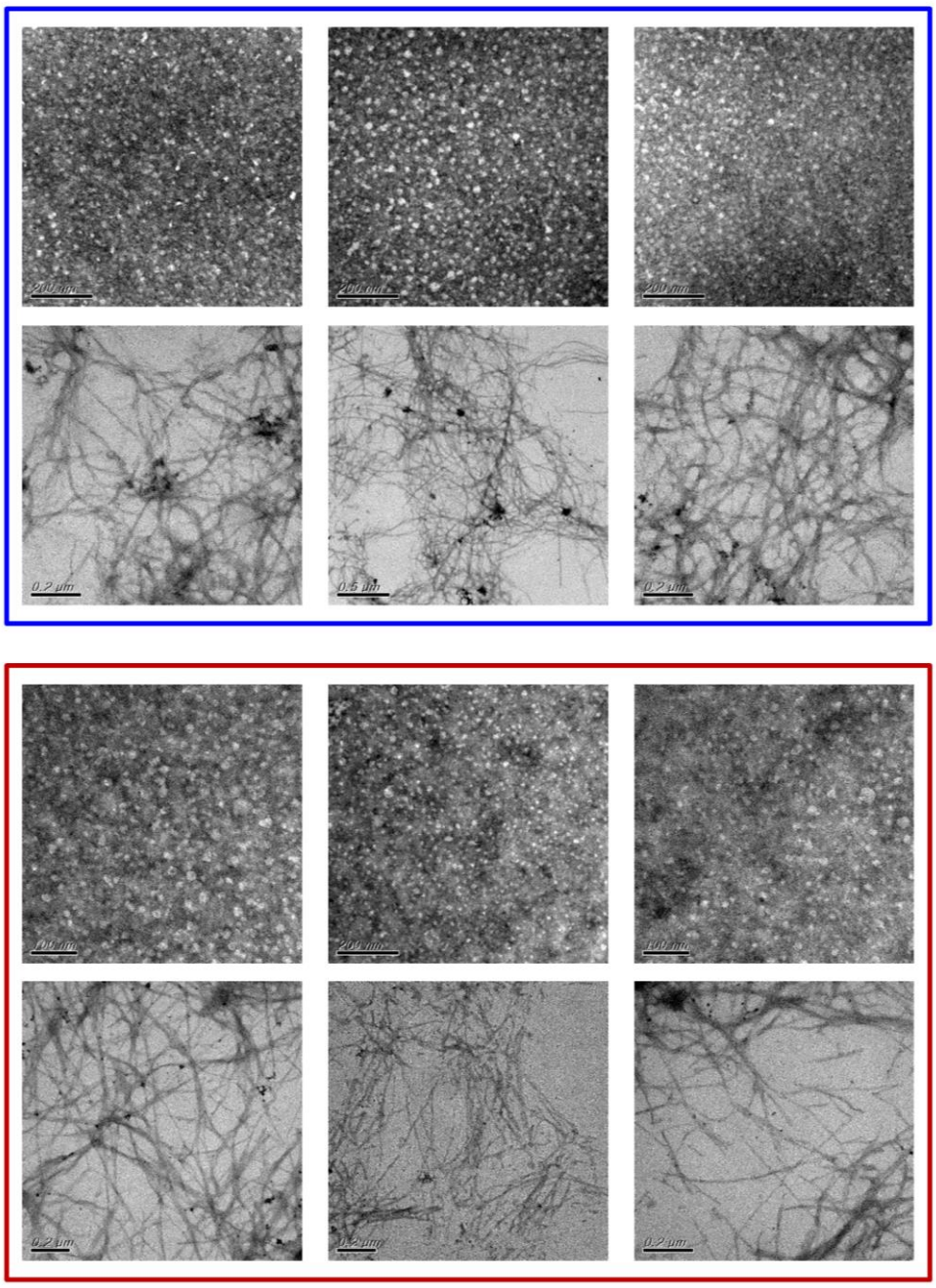

Fig. S9. Typical TEM images of the samples of $RM_{CO520}Aβ_{40}$ (red frame) and $RM_{CO520}Aβ_{42}$ (blue frame). For each frame, the images on the upper row show the sample morphology right after back extraction and those on the lower row correspond to the sample after prolonged incubation. These images confirmed that the fibril formation occurred via self aggregation of $RM_{CO520}Aβ$.

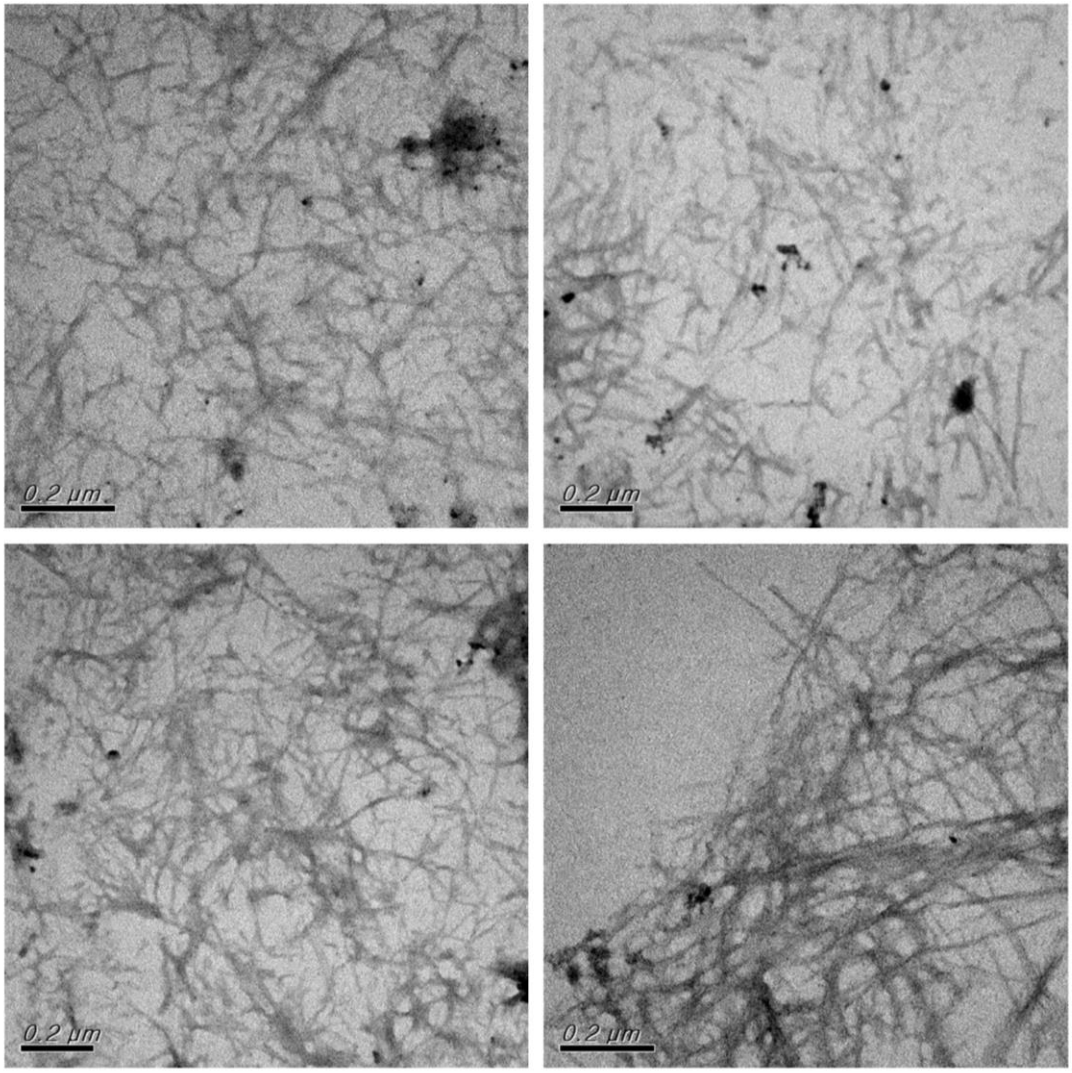

Fig. S10. Typical TEM images of the fibrils formed by the self-aggregation of $RM_{CO520}A\beta_{42/40}$.

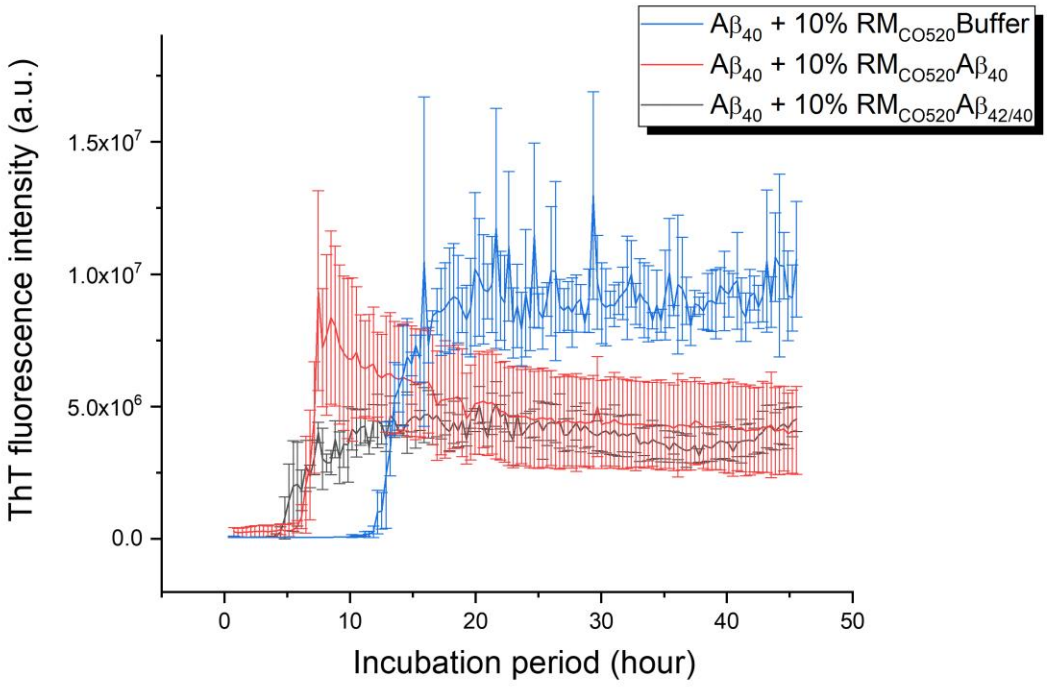

Fig. S11. ThT fluorescence results for probing the seeding effects of $RM_{CO520}A\beta_{42/40}$. The data of $RM_{CO520}A\beta_{40}$ and RM_{CO520}Buffer (sample prepared in the absence of Aβ peptides) were shown as positive and negative controls, respectively.

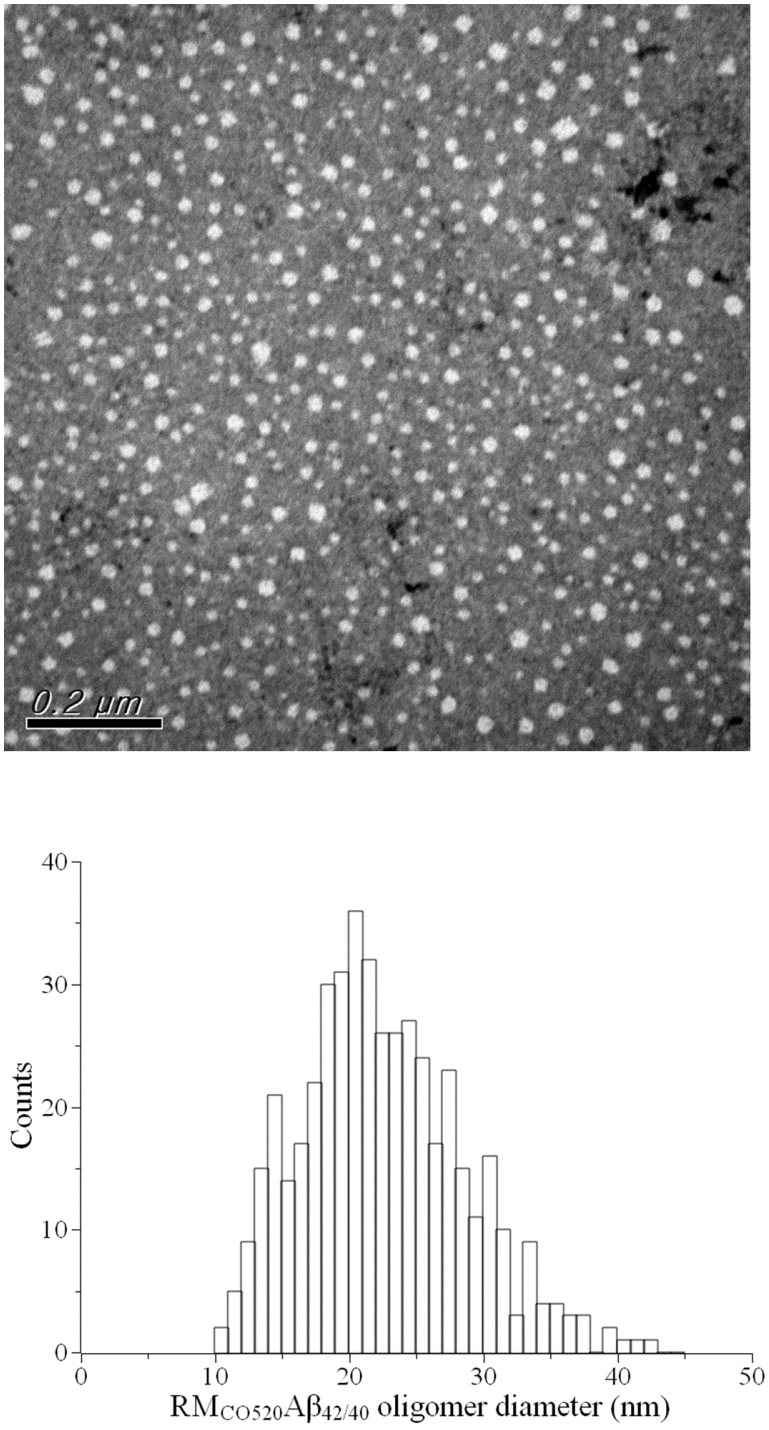

Fig. S12. Negatively stained TEM image of $RM_{CO520}A\beta_{42/40}$. Size distribution of the spherical aggregates, where the statistical analysis of the data comprising 460 particles gave an average size of 22.5 ± 6.1 nm.

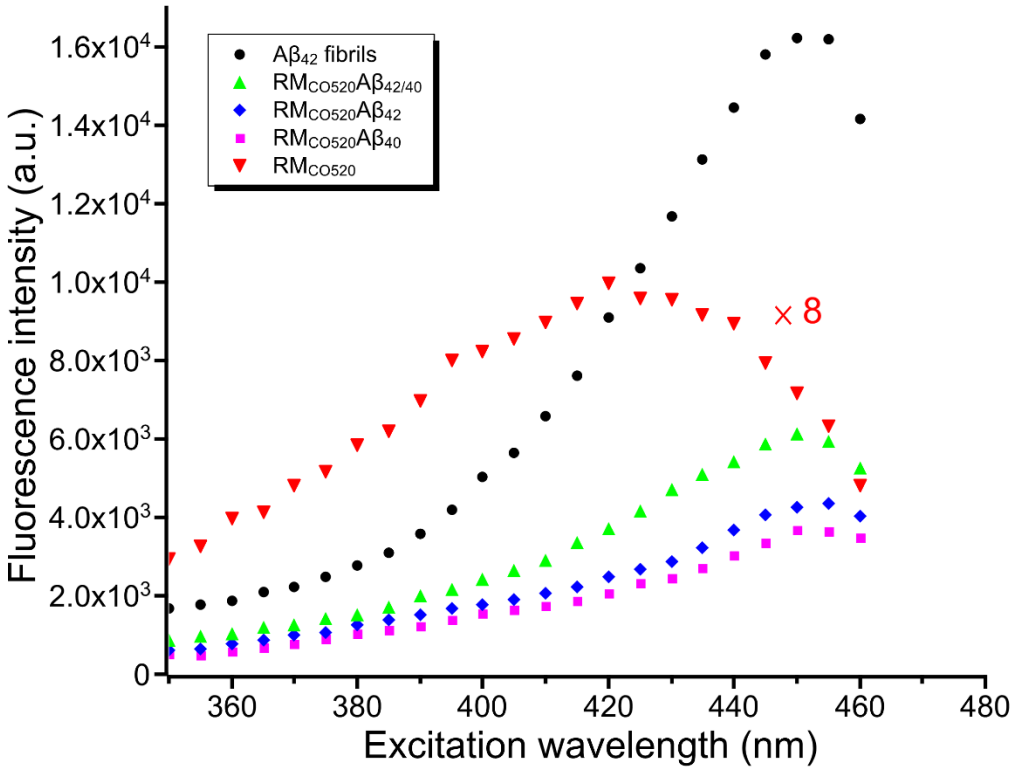

Fig. S13. ThT excitation profile for $RM_{CO520}A\beta$. The excitation wavelength was swept from 350 to 460 nm, while the fluorescence intensity at 490 nm was monitored. The $A\beta_{42}$ fibrils and the RM_{CO520} sample were taken as the positive and negative controls, respectively. The intensity of the RM_{CO520} had been multiplied by 8 times. The shifts in λ_{max} indicate that ThT molecules can bind to all the $RM_{CO520}A\beta$ samples.

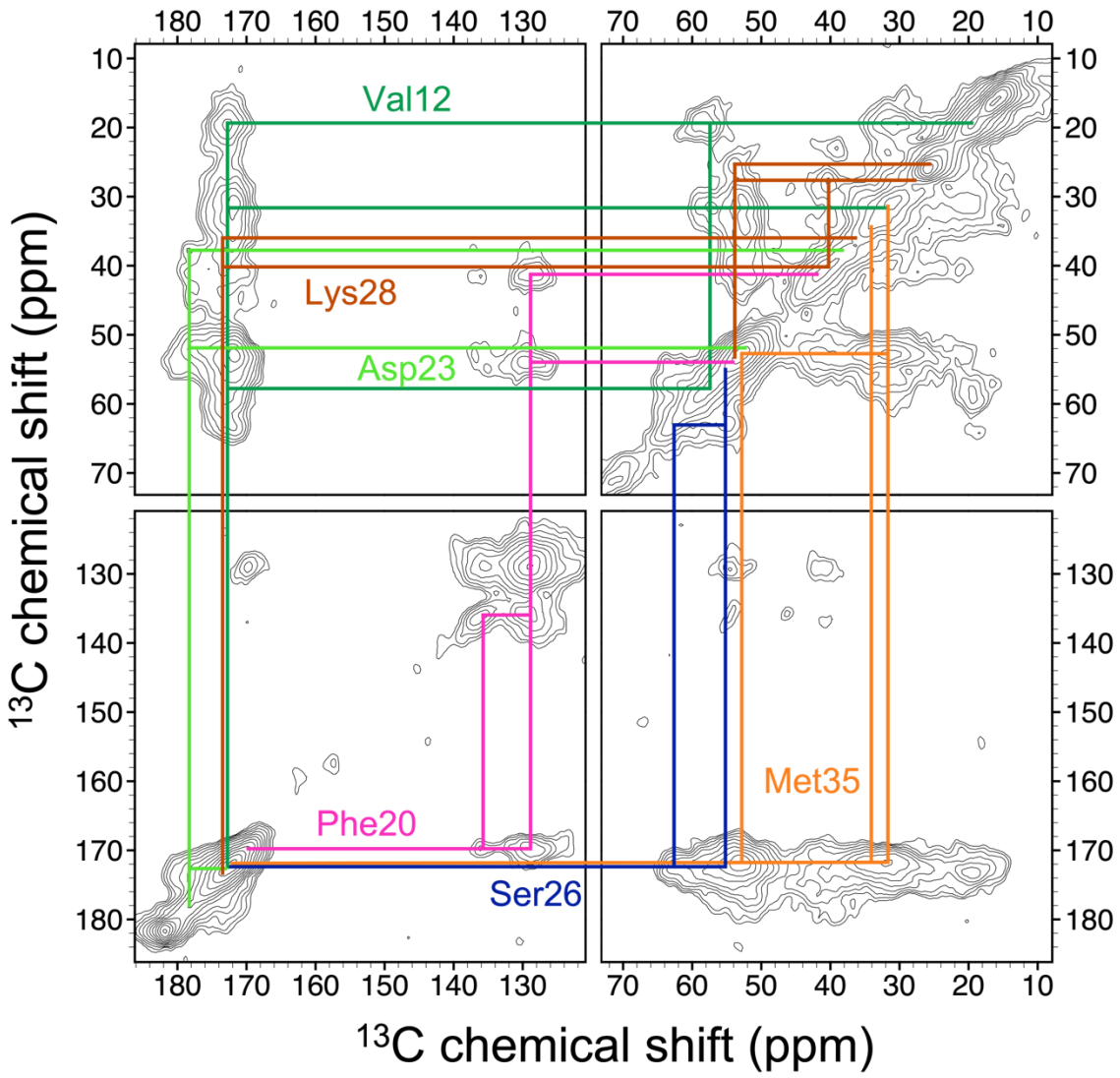

Fig. S14. Spectral assignment for the ^{13}C homonuclear correlation spectrum of $RM_{CO520}A\beta_{40}$ with S2 labeling scheme. The processing parameters are given in Materials and Methods.

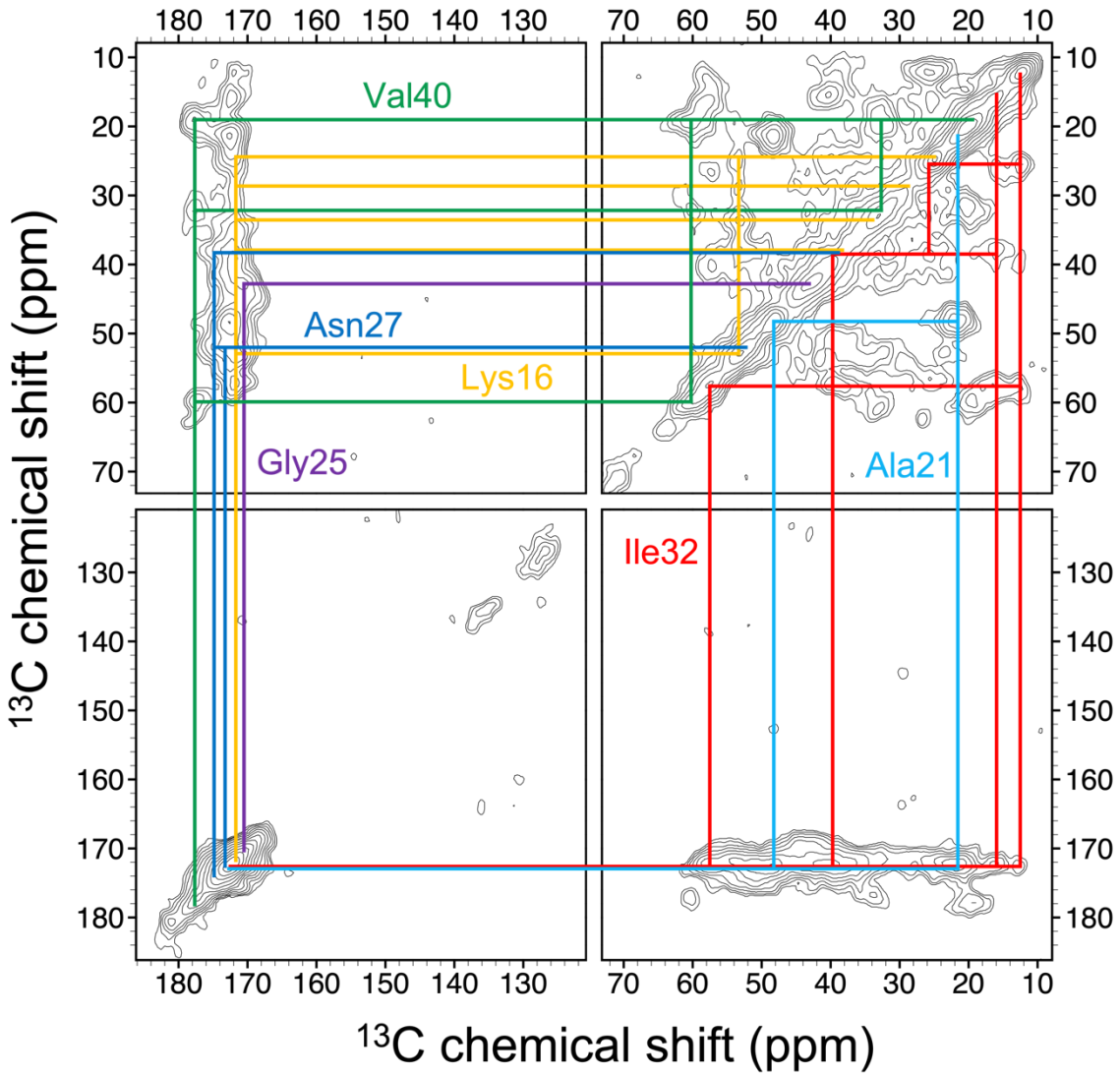

Fig. S15. Spectral assignment for the ^{13}C homonuclear correlation spectrum of $RM_{CO520}A\beta_{40}$ with S3 labeling scheme.

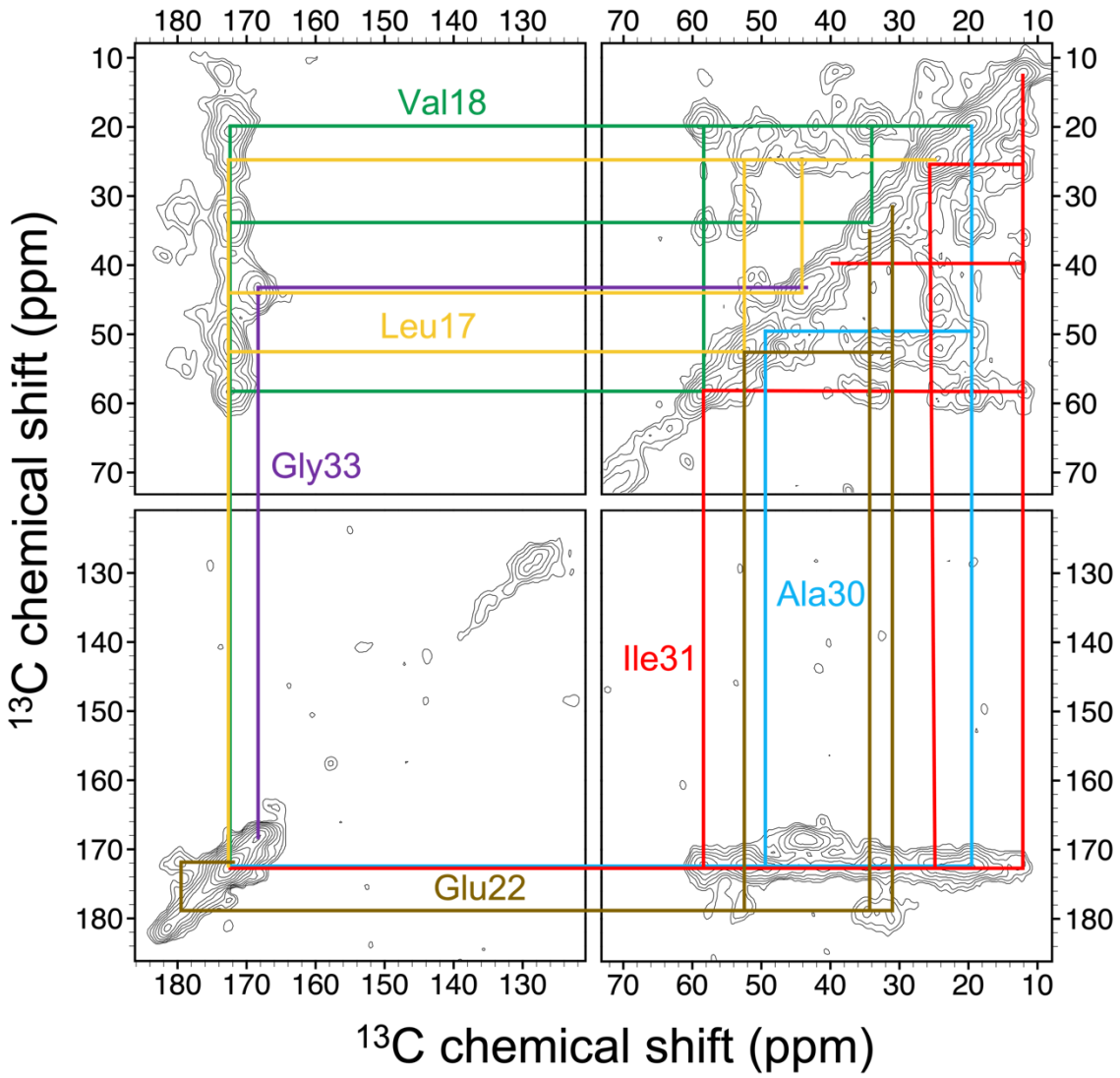

Fig. S16. Spectral assignment for the ^{13}C homonuclear correlation spectrum of $RM_{CO520}A\beta_{40}$ with S4 labeling scheme.

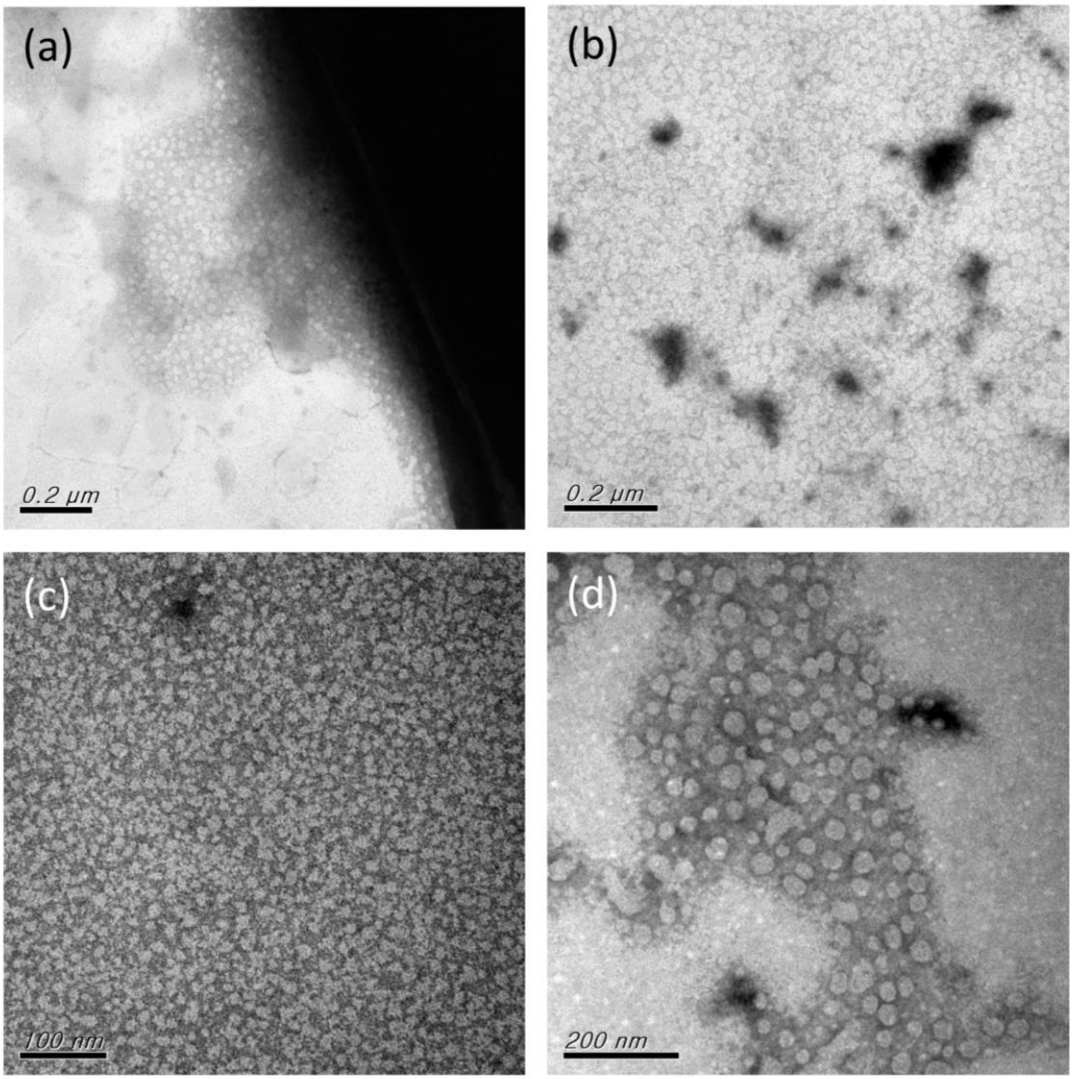

Fig. S17. TEM images of the samples after NMR measurements: (a,b) $RM_{CO520}A\beta_{40}$; (c, d) $RM_{CO520}A\beta_{42/40}$

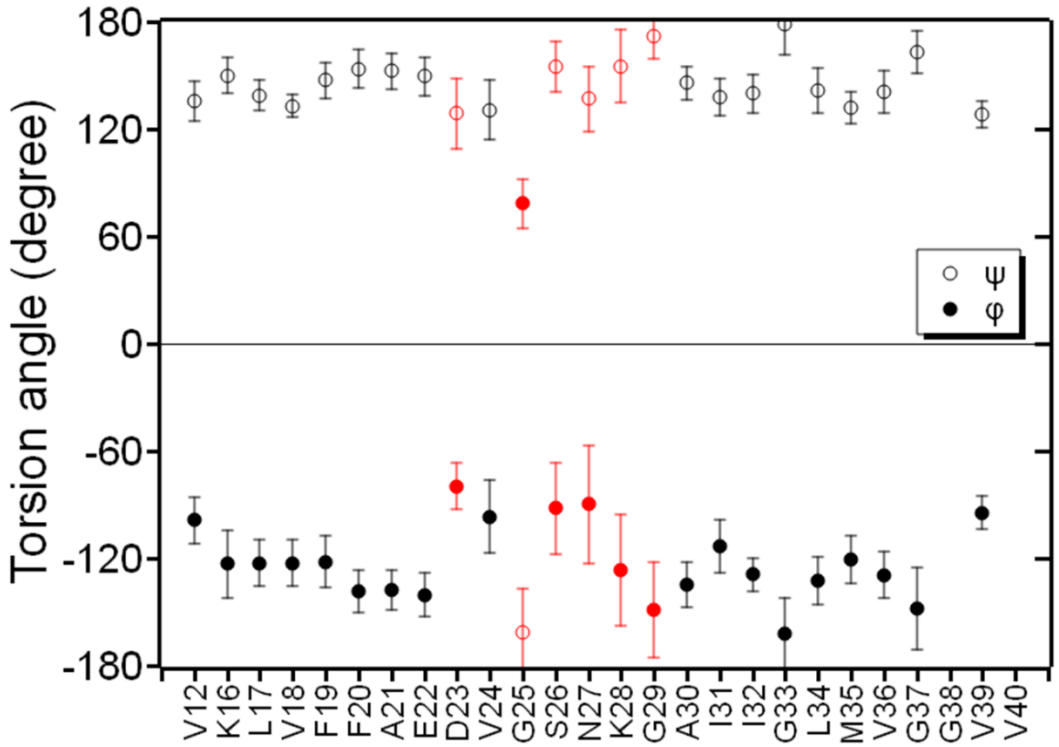

Fig. S18. Dihedral angles (ϕ, ψ) estimated by TALOS-N analysis for $RM_{CO520}A\beta_{40}$. The data points in red belong to the "Warn" class, which were considered to be less reliable. The rest are all in the "Strong" class.

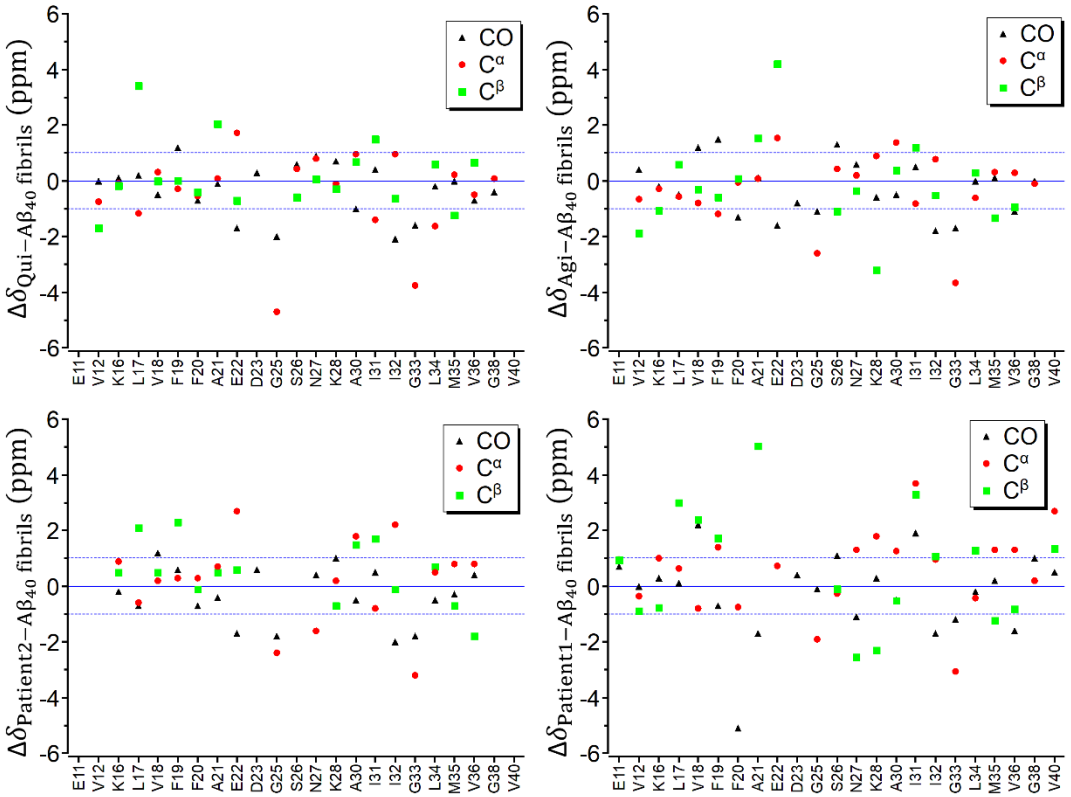

Fig. S19. ^{13}C chemical shift deviation between $RM_{CO520}A\beta_{40}$ and various $A\beta_{40}$ fibrils.

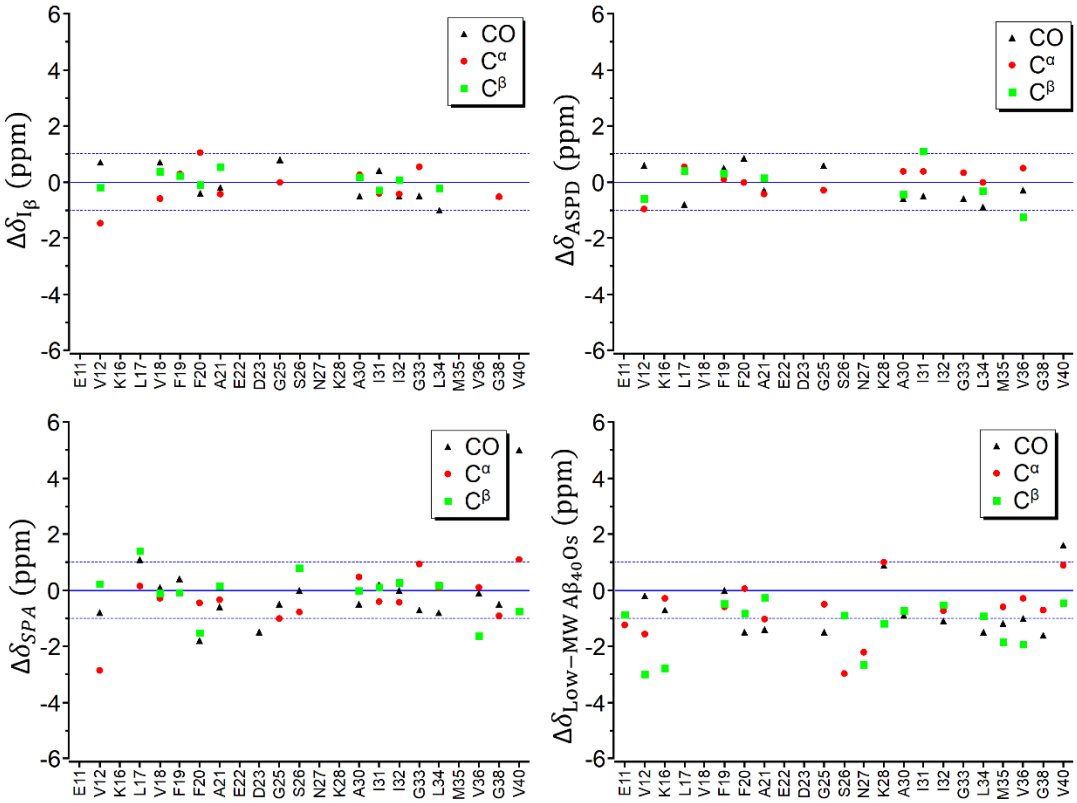

Fig. S20. ^{13}C chemical shift deviation between $RM_{CO520}A\beta_{40}$ and various Aβ oligomers.

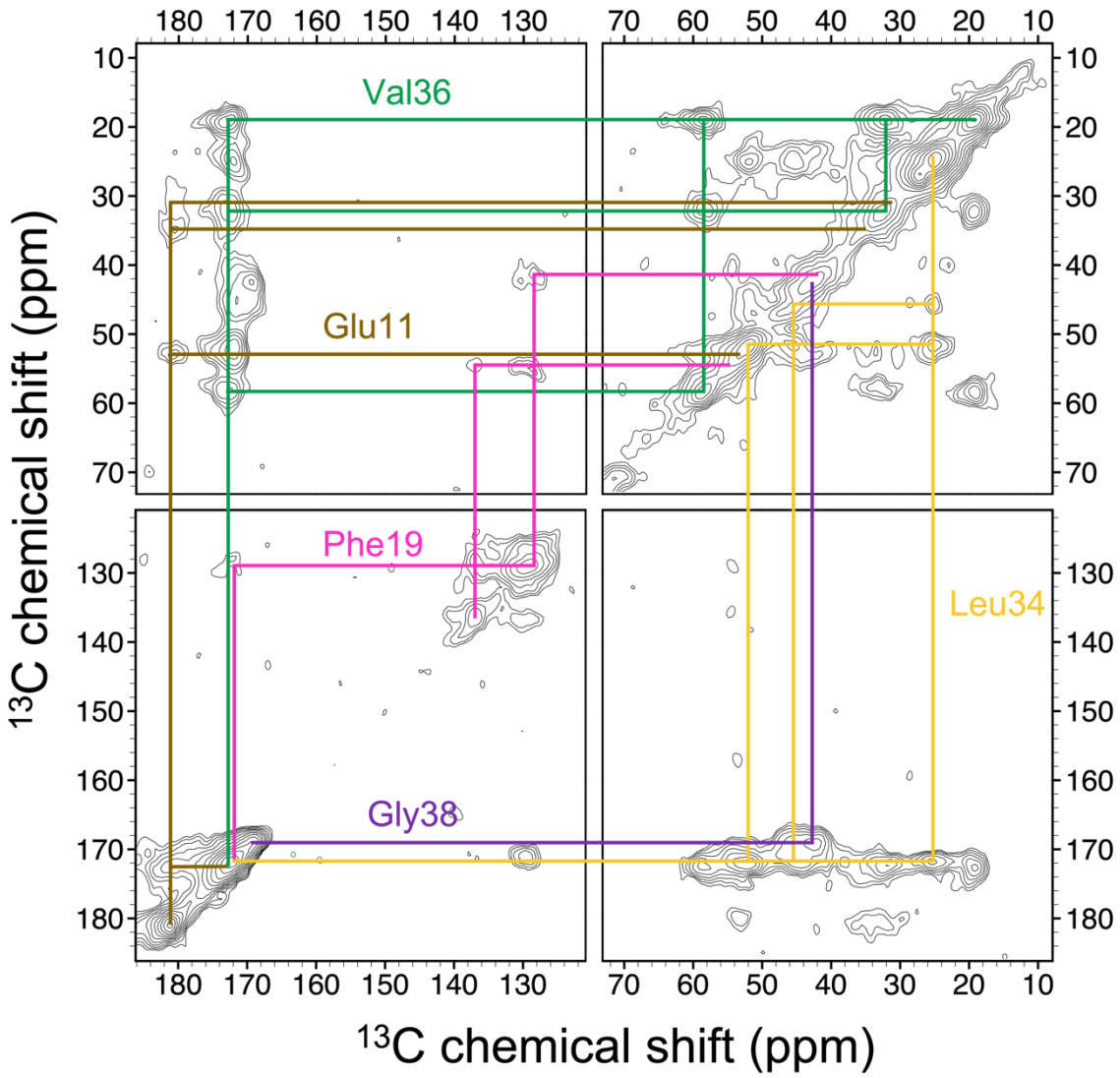

Fig. S21. Spectral assignment for the ^{13}C homonuclear correlation spectrum of $RM_{CO520}A\beta_{42/40}$ with S1 labeling scheme.

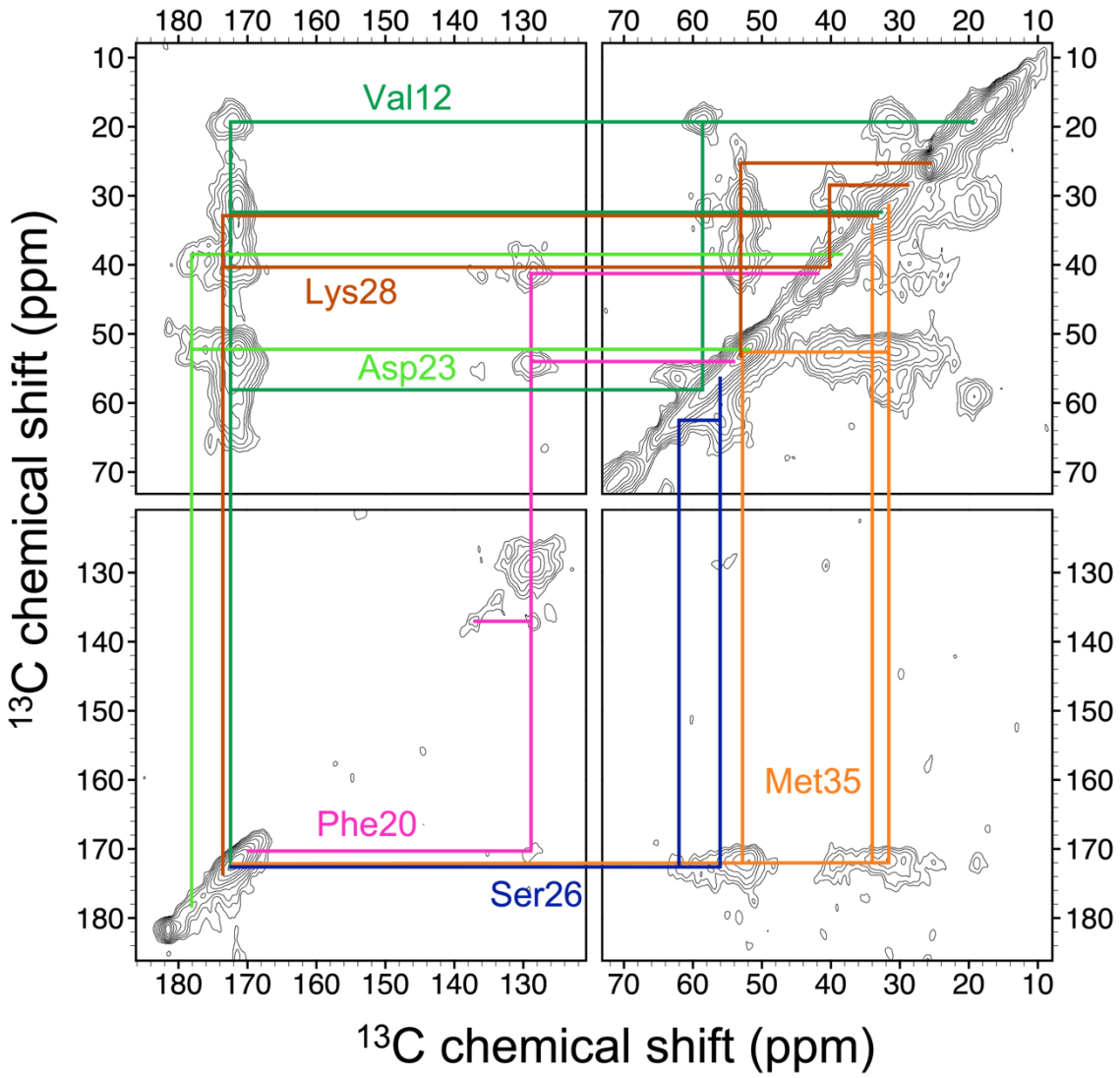

Fig. S22. Spectral assignment for the ^{13}C homonuclear correlation spectrum of $RM_{CO520}A\beta_{42/40}$ with S2 labeling scheme.

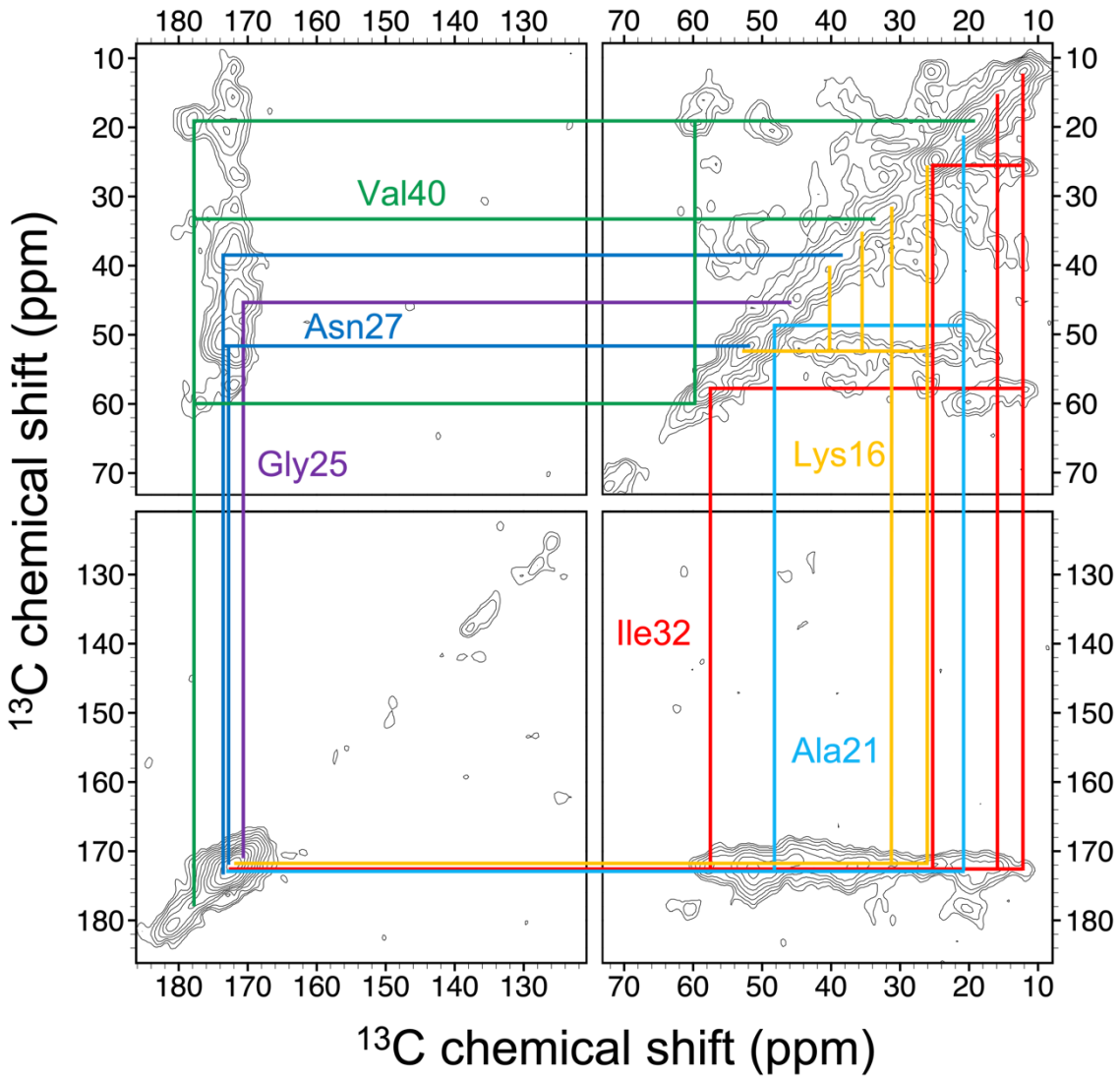

Fig. S23. Spectral assignment for the ^{13}C homonuclear correlation spectrum of $RM_{CO520}A\beta_{42/40}$ with S3 labeling scheme.

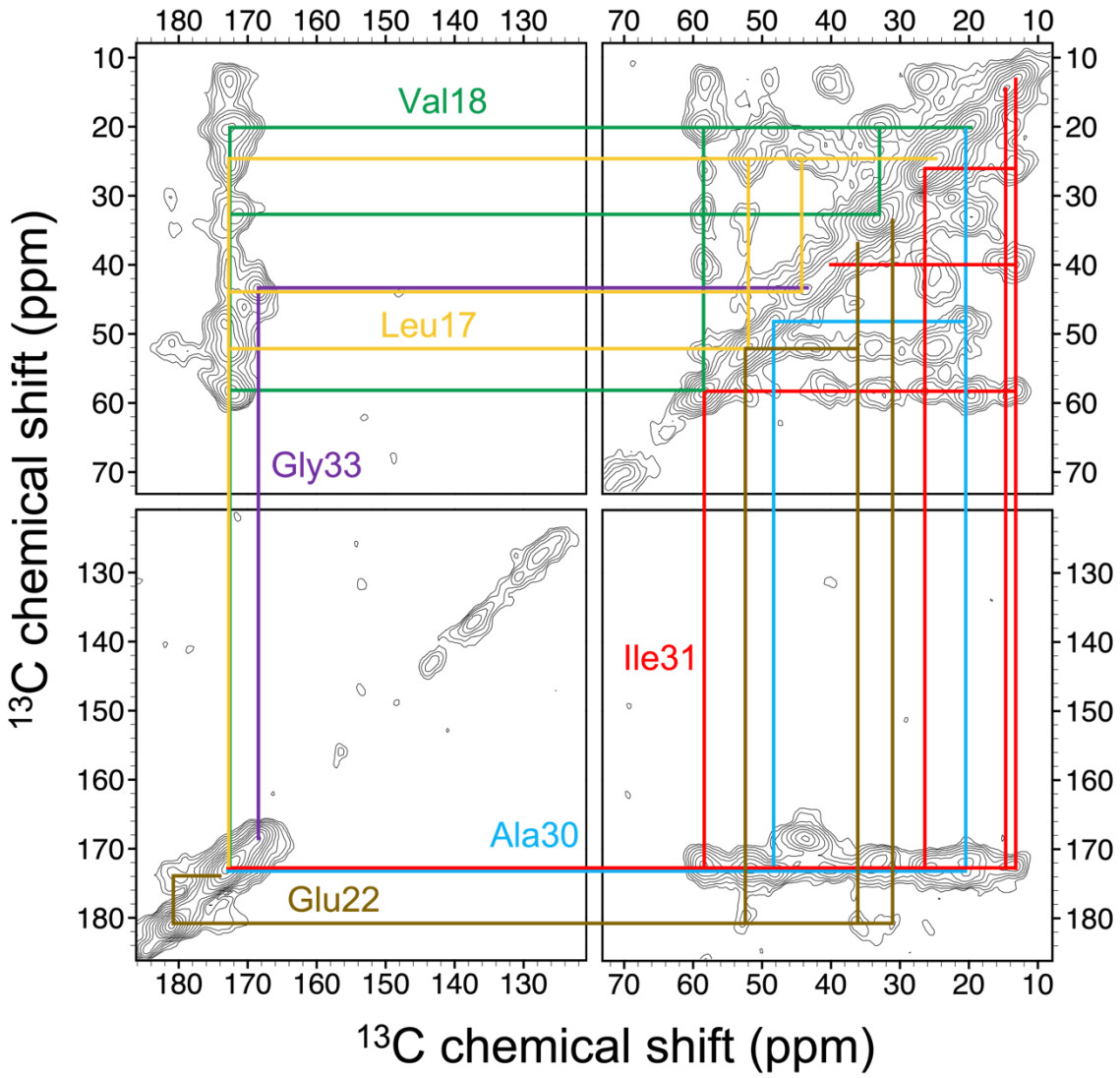

Fig. S24. Spectral assignment for the ^{13}C homonuclear correlation spectrum of $RM_{CO520}A\beta_{42/40}$ with S4 labeling scheme.

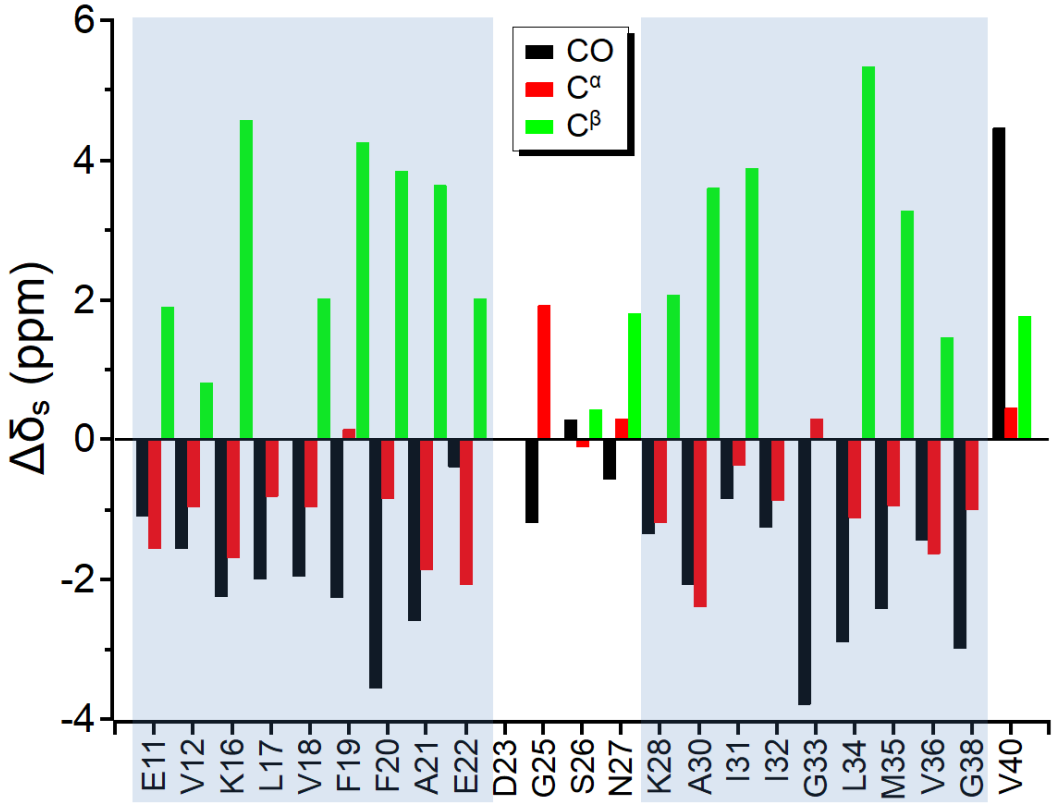

Fig. S25. Secondary chemical shift ($\Delta\delta_s$) of $RM_{CO520}A\beta_{42/40}$. $\Delta\delta_s = \delta - \delta_{rand}$, where δ_{rand} denotes the random coiled values.

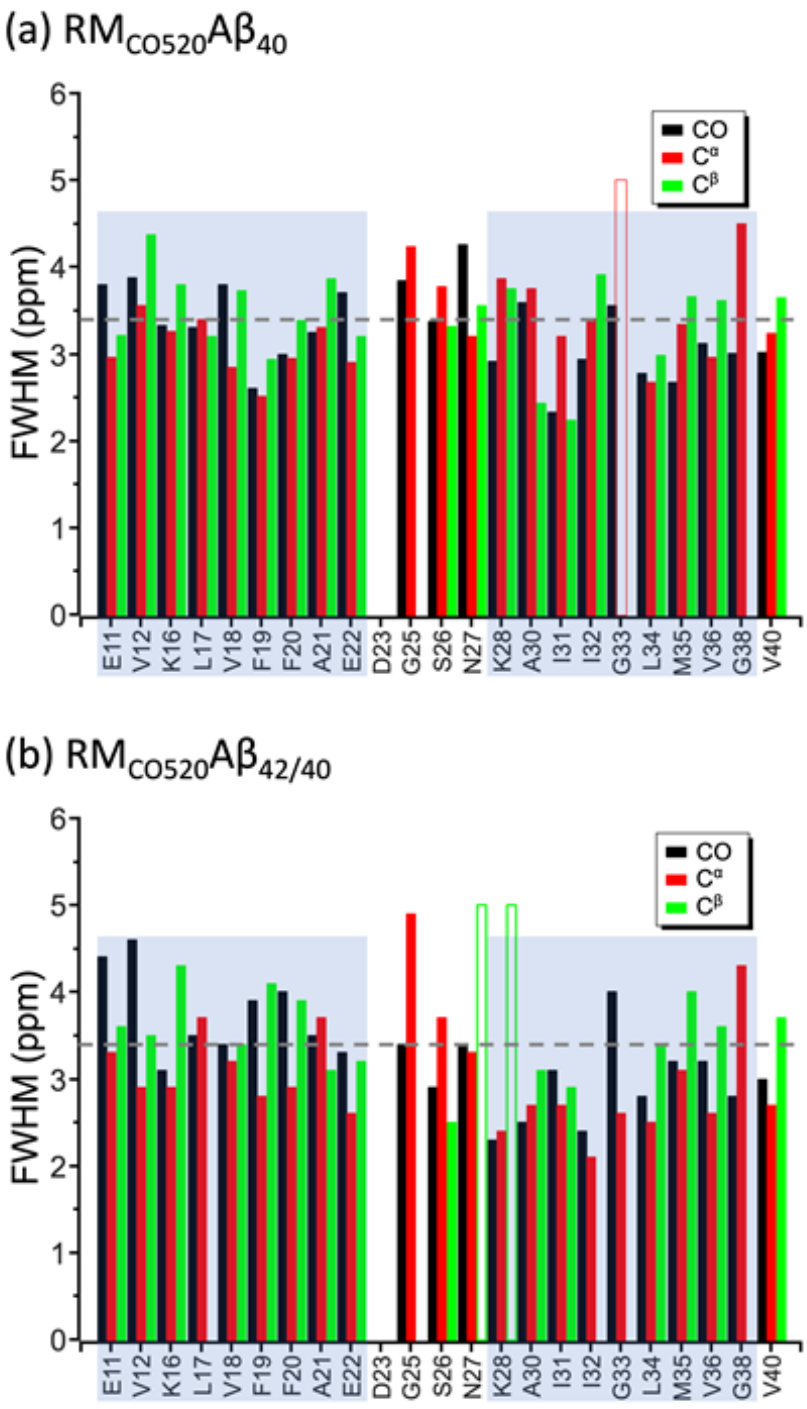

Fig. S26. Full width at half maximum (FWHM) data for **(a)** $RM_{CO520}A\beta_{40}$ and **(b)** $RM_{CO520}A\beta_{42/40}$. The FWHM data of D23 and I32-C^{β} for $RM_{CO520}A\beta_{42/40}$ were not determined due to the limited spectral resolution. The dashed lines denote the average FWHM. The open bars denote FWHM > 5 ppm.

(a)

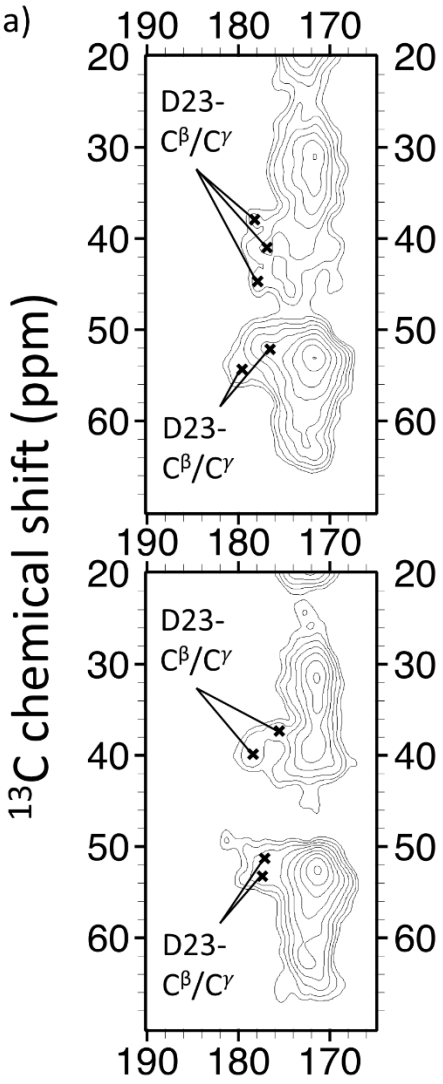

(b)

	CO	Cα	Cβ	Cγ	Cδ	Cε
E11		##	##	##		
V12						
H13						
H14						
Q15						
K16		##		##		
L17			##			
V18						
F19		###	##		###	
F20		**		**	**	
A21		##	##			
E22	##	** ##	** ##	##	** ##	
D23		** ##	*** ##	***** ####		
V24						
G25						
S26						
N27						
K28						
G29						
A30		**	**			
I31						
I32		##		##	##	
G33						
L34						
M35						
V36						
G37						
G38						
V39						
V40						

Fig. S27. (a) The cross-peak patterns of the D23-C^{β}/C^{γ} for $RM_{CO520}A\beta_{40}$ (top) and $RM_{CO520}A\beta_{42/40}$ (bottom). No major peaks can be identified **(b)** Schematic illustration of the difference in ^{13}C chemical shifts ($\Delta\delta$) between $RM_{CO520}A\beta_{42/40}$ and $RM_{CO520}A\beta_{40}$ with the color code of: cyan, $\Delta\delta \leq 0.5$ ppm; pink, 0.5 ppm $< \Delta\delta \leq 1.0$ ppm; magenta, $\Delta\delta > 1.0$ ppm. The boxes in red indicate that the data for $RM_{CO520}A\beta_{42/40}$ and $RM_{CO520}A\beta_{40}$ cannot be compared due to the lack of major peaks. The boxes in grey denote data unmeasured or could not be determined. The number of multiple peaks, if any, was indicated by the number of # and * for $RM_{CO520}A\beta_{42/40}$ and $RM_{CO520}A\beta_{40}$, respectively.

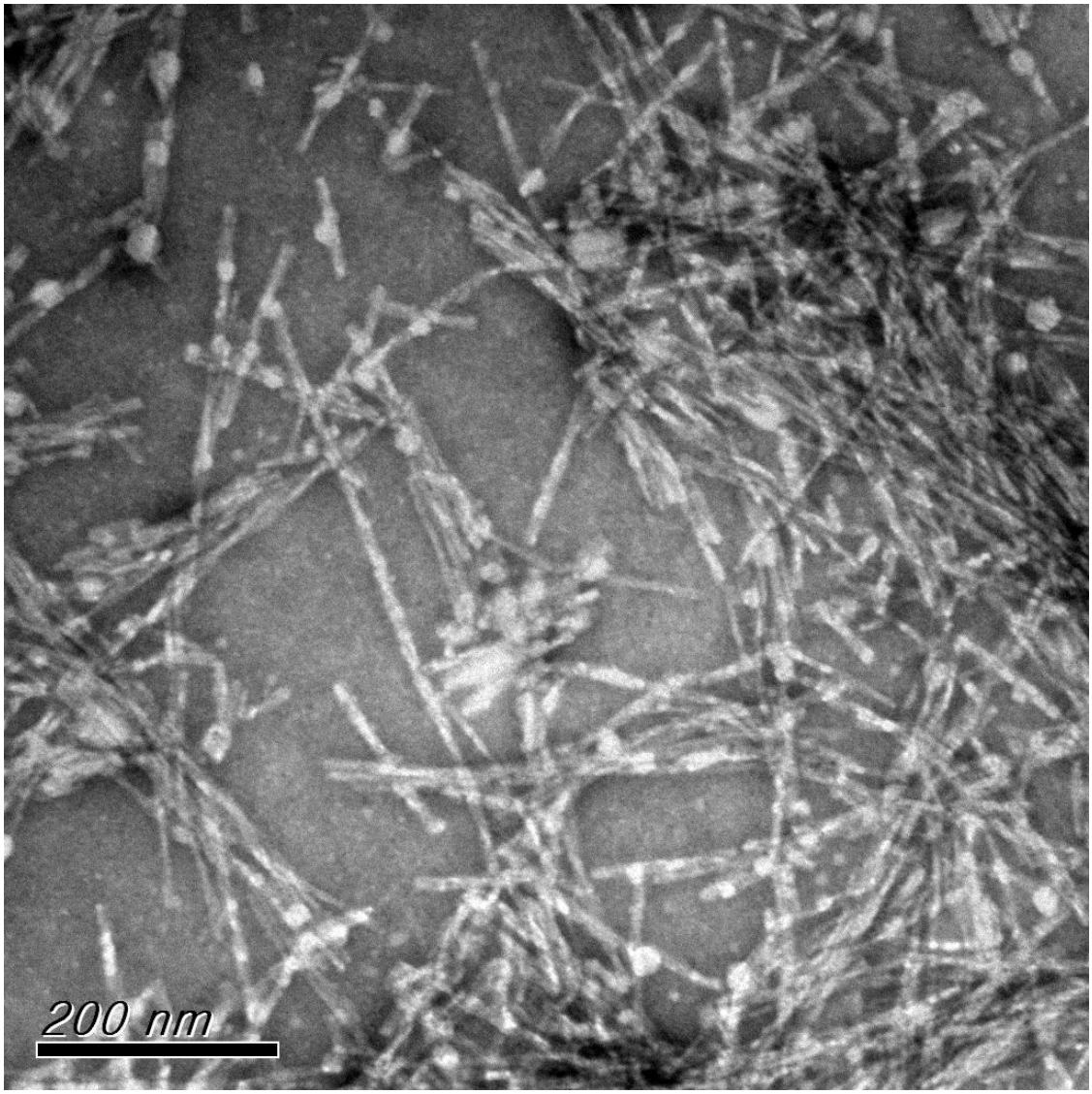

Fig. S28. Typical TEM image of $RM_{CO520}A\beta_{42/40}$ fibrils formed by incubating the isotopically enriched $RM_{CO520}A\beta_{42/40}$ oligomers.

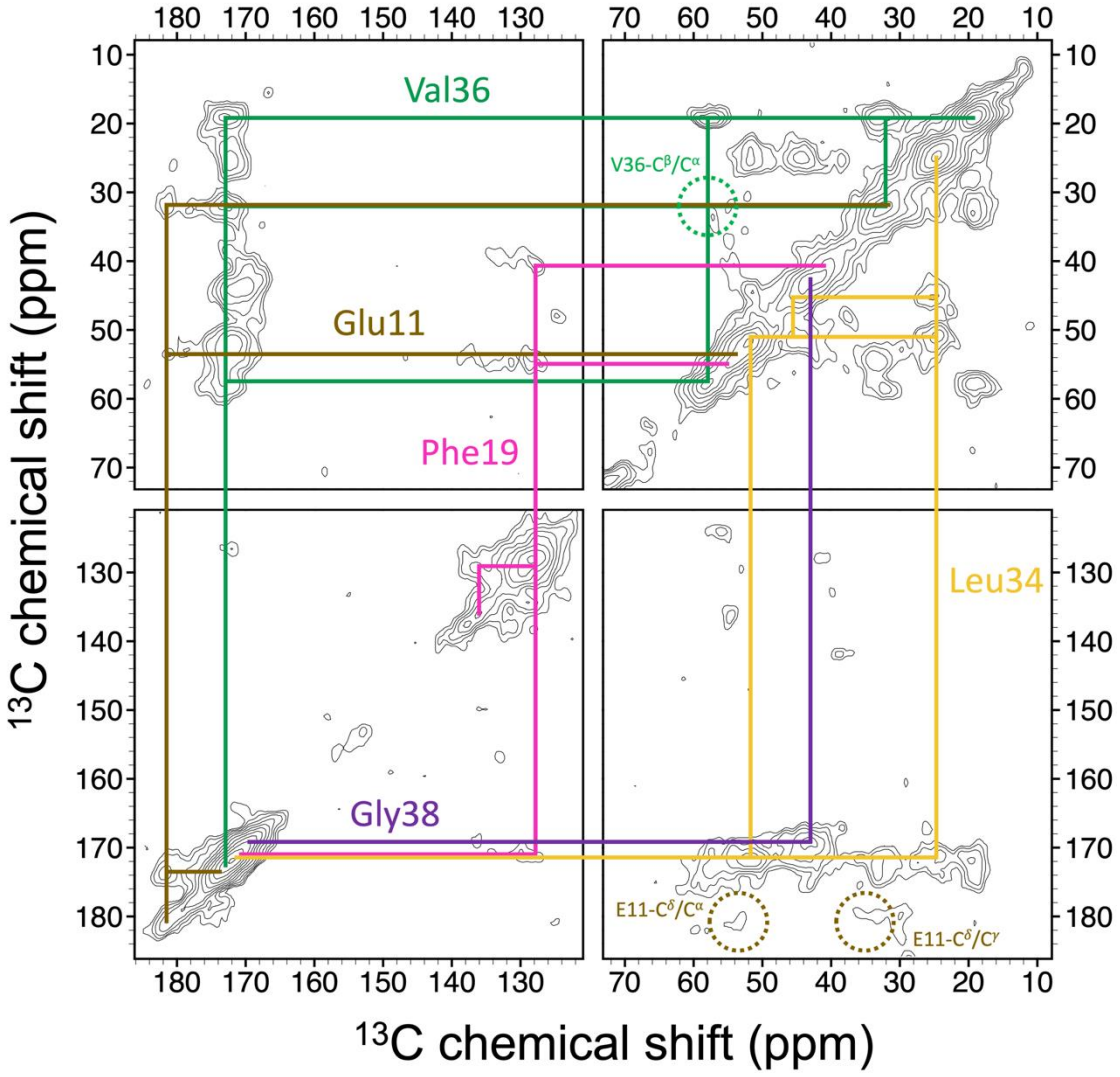

Fig. S29. Spectral assignment for the ^{13}C homonuclear correlation spectrum of $RM_{CO520}A\beta_{42/40}$ fibrils with S1 labeling scheme. The dotted circles highlight the positions at which more intensive cross peaks were observed for the $RM_{CO520}A\beta_{42/40}$ oligomers.

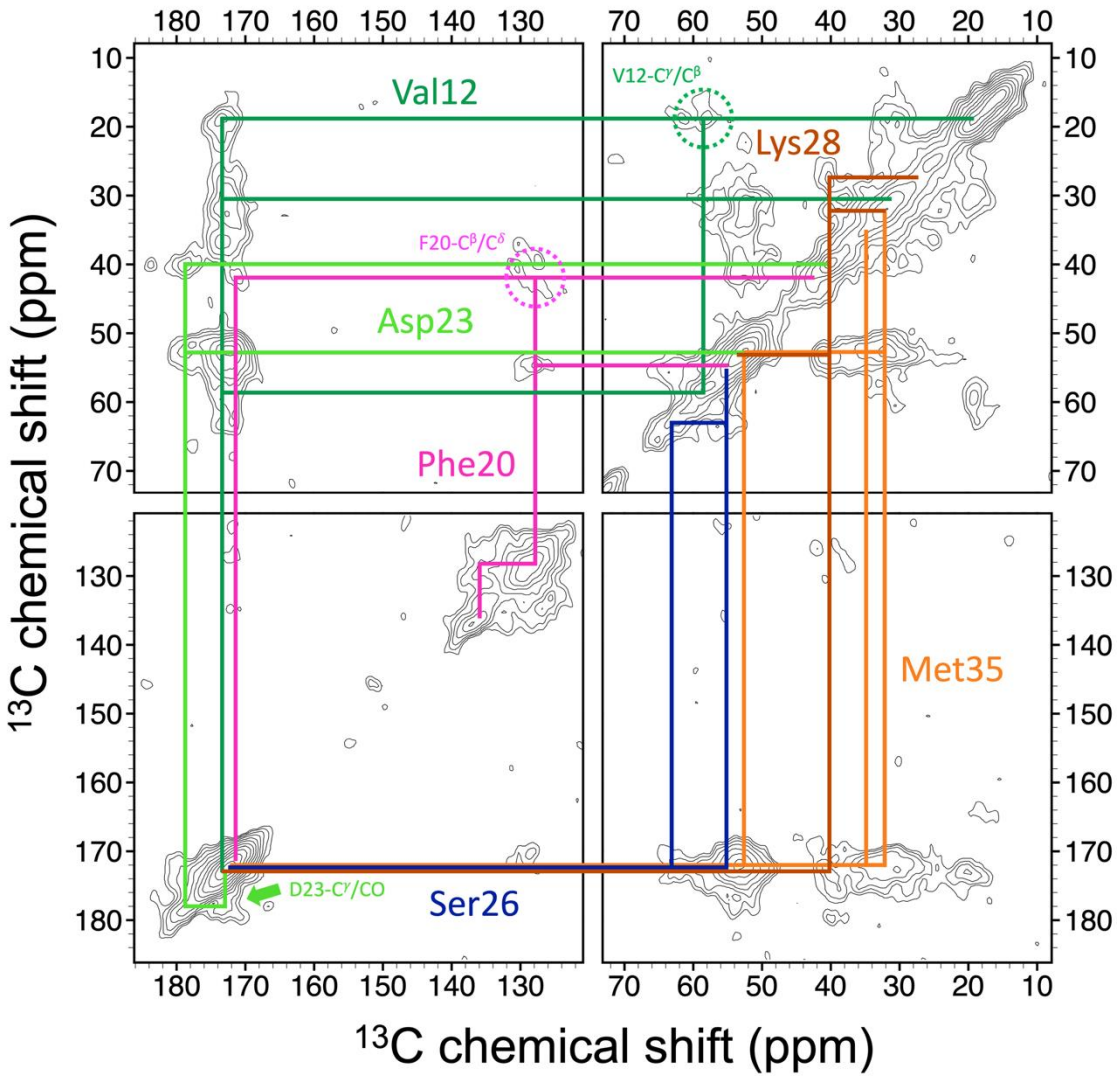

Fig. S30. Spectral assignment for the ^{13}C homonuclear correlation spectrum of $RM_{CO520}A\beta_{42/40}$ fibrils with S2 labeling scheme. The dotted circles highlight the positions at which more intensive cross peaks were observed for the $RM_{CO520}A\beta_{42/40}$ oligomers. The arrows indicate the cross peaks which are more intensive than the corresponding signals of the oligomers.

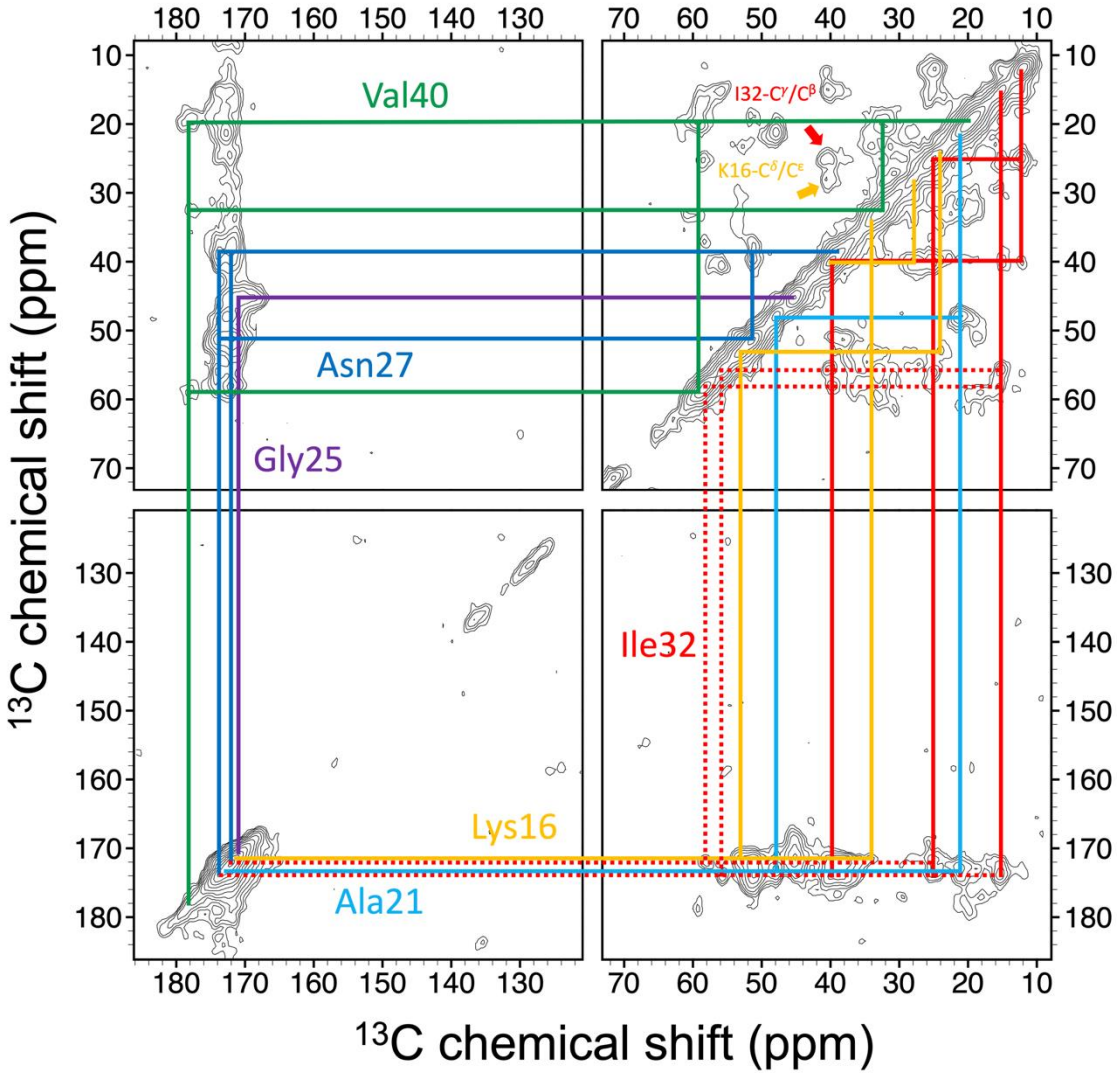

Fig. S31. Spectral assignment for the ^{13}C homonuclear correlation spectrum of $RM_{CO520}A\beta_{42/40}$ fibrils with S3 labeling scheme. The spectrum was acquired at a magnetic field of 14.1 T. The arrows indicate the cross peaks which are more intensive than the corresponding signals of the oligomers.

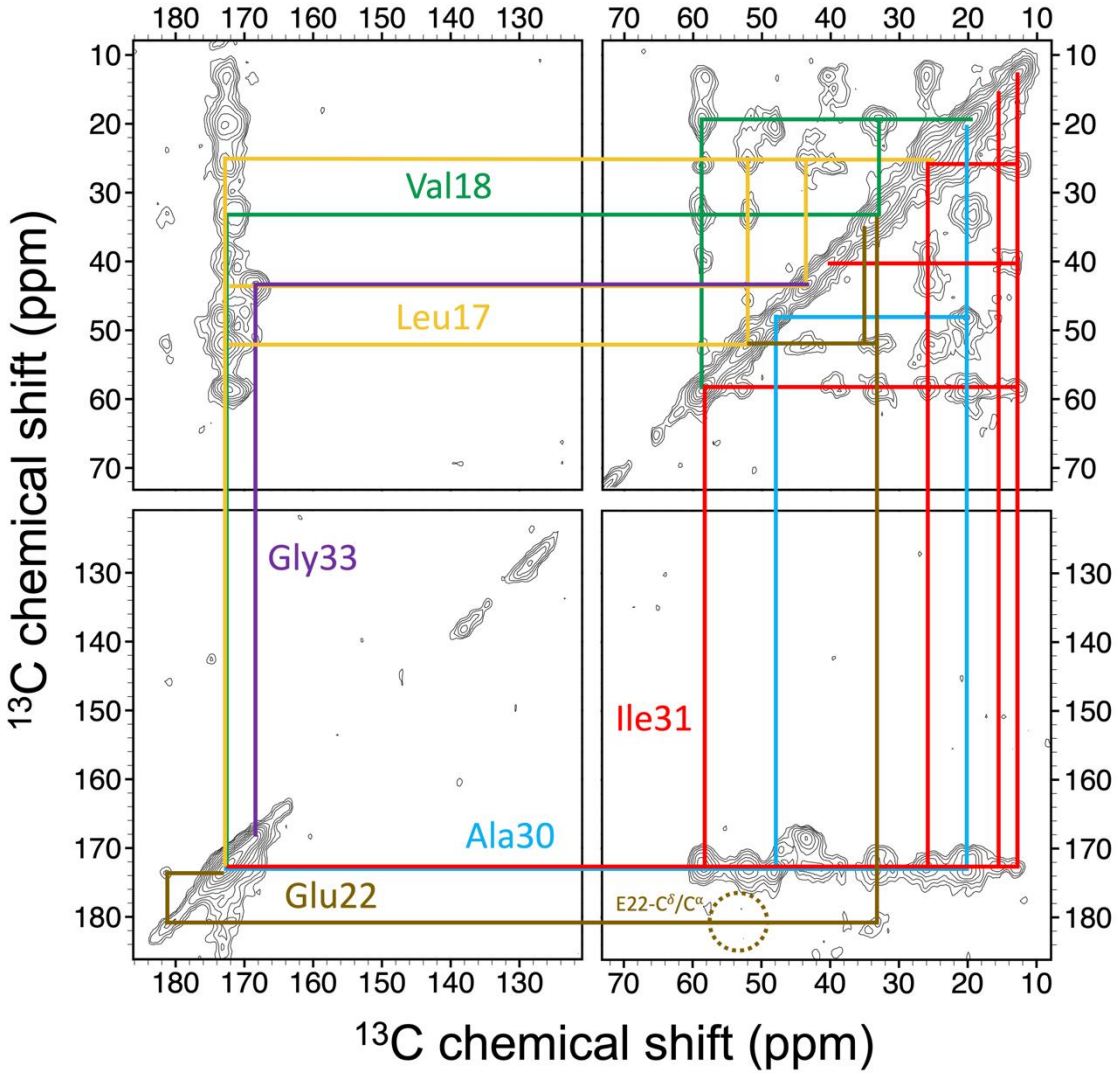

Fig. S32. Spectral assignment for the ^{13}C homonuclear correlation spectrum of $RM_{CO520}A\beta_{42/40}$ fibrils with S4 labeling scheme. The spectrum was acquired at a magnetic field of 14.1 T. The dotted circles highlight the positions at which more intensive cross peaks were observed for the $RM_{CO520}A\beta_{42/40}$ oligomers.

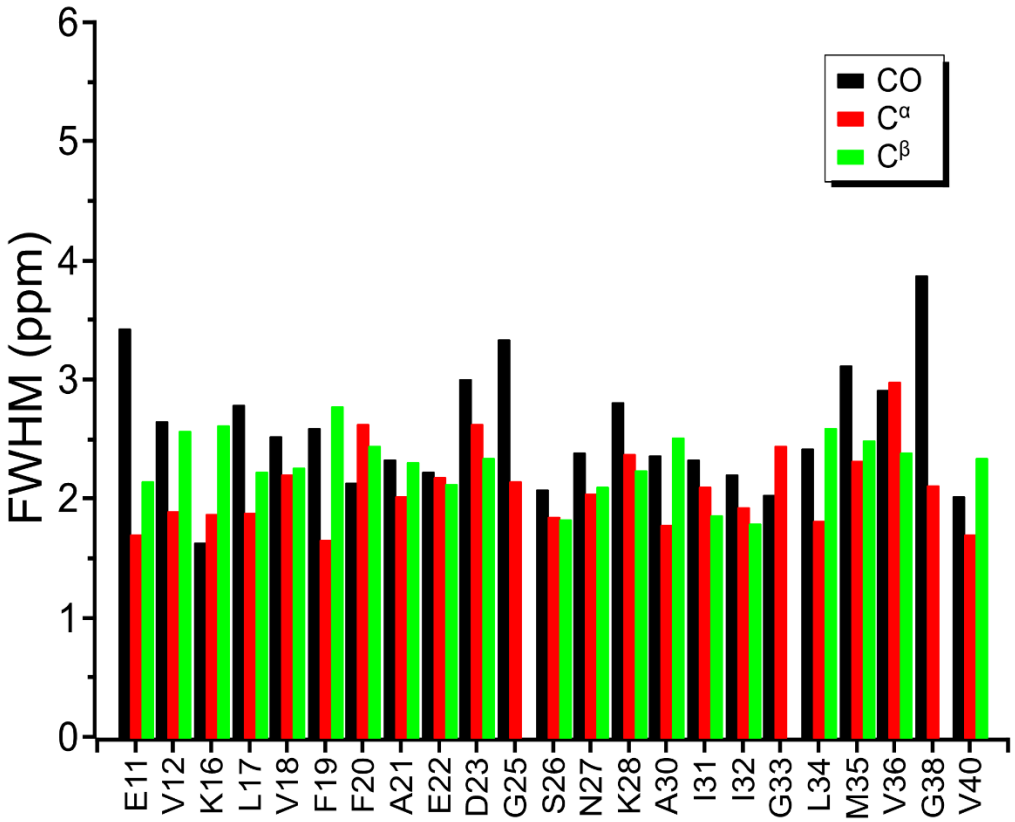

Fig. S33. Full width at half maximum (FWHM) data for $RM_{CO520}A\beta_{42/40}$ fibrils.

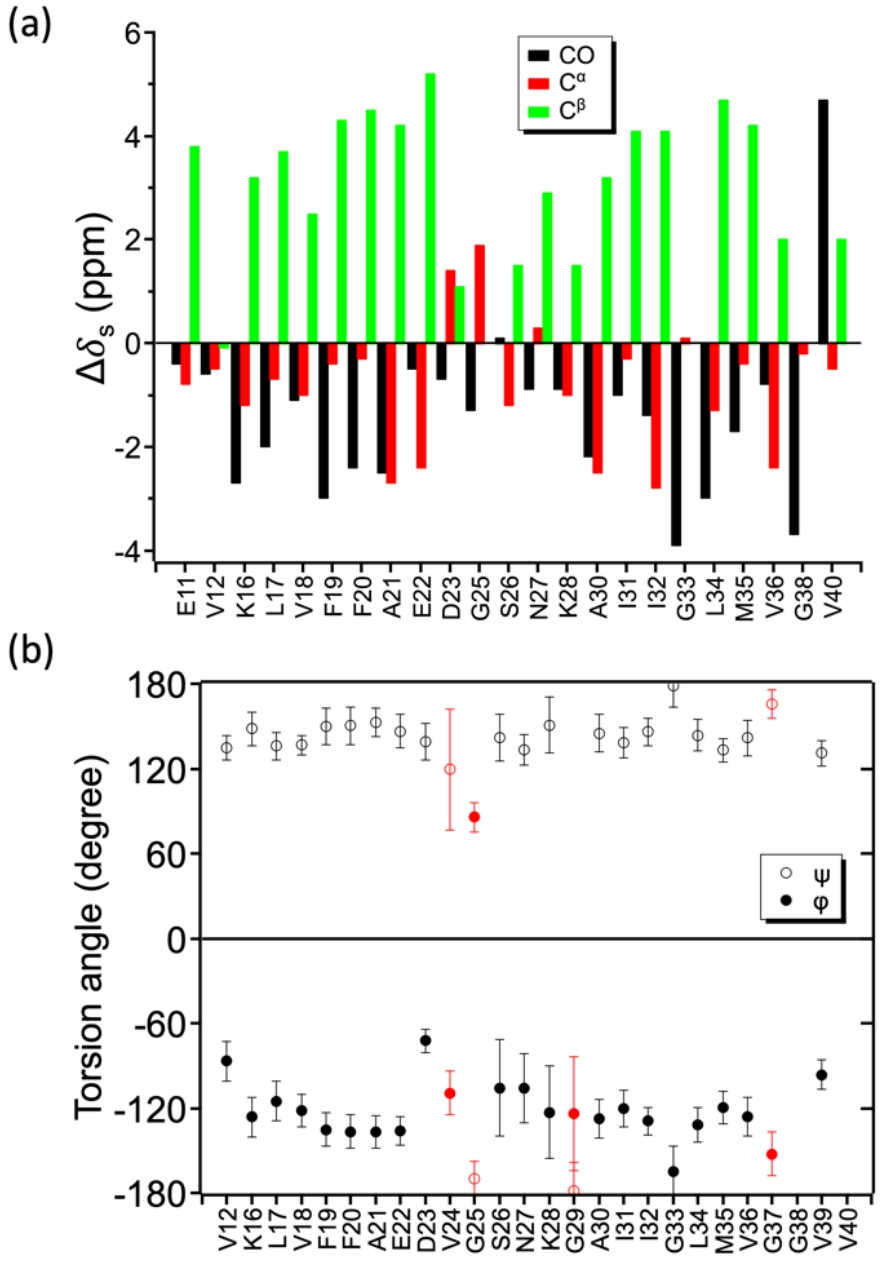

Fig. S34. (a) Secondary chemical shift ($\Delta\delta_s$) of $RM_{CO520}A\beta_{42/40}$ fibrils. $\Delta\delta_s = \delta - \delta_{rand}$, where δ_{rand} denotes the random coiled values. **(b)** Dihedral angles (ϕ, ψ) estimated by TALOS-N analysis for $RM_{CO520}A\beta_{42/40}$ fibrils. The data points in red belong to the "Warn" class, which were considered to be less reliable. The rest are all in the "Strong" class.

Tables

Table S1. EA data for RM_{CO520}-$A\beta_{40}$ samples.[1]

Species/Measurement	Mass (mg)	N (%)	C (%)	S (%)	H (%)
$A\beta_{40}$	--	17.1	53.8	0.74	6.9
CO520	--	0	68.1	0	10.0
1	4.067	4.277	28.695	0.674	5.307
2	3.704	4.785	28.698	0.394	5.196
3	3.170	4.728	29.204	0.434	5.319
4	3.141	3.864	31.358	0.202	4.959
5	3.564	4.093	28.206	0.209	4.496
6	3.113	4.198	26.569	0.234	4.512

[1] Molecular formulae of $A\beta_{40}$ and CO520 are $C_{194}H_{295}N_{53}O_{58}S$ (4329.8 g/mol) and $C_{25}H_{44}O_6$ (MW 440.6 g/mol), respectively.

$$\chi \equiv \sum_{i=1}^{6} \Big\{ \big(\%(A\beta_{40}) \times 0.171 - \%N_{\mathrm{exp},i}\big)^2 + \big(\%(A\beta_{40}) \times 0.538 + \%(\mathrm{CO520}) \times 0.681 - \%C_{\mathrm{exp},i}\big)^2 + \big(\%(A\beta_{40}) \times 0.0074 - \%S_{\mathrm{exp},i}\big)^2 + \big(\%(A\beta_{40}) \times 0.069 + \%(\mathrm{CO520}) \times 0.10 - \%H_{\mathrm{exp},i}\big)^2 \Big\}$$

Table S2. Labeling scheme for the ^{13}C enriched $RM_{CO520}A\beta_{40}$ sample.

S1	DAEFRHDSGY **E**VHHQKLV**F**F AEDVGSNKGA IIG**L**M**V**G**G**VV
S2	DAEFRHDSGY E**V**HHQKLVF**F** AE**D**VG**S**N**K**GA IIGL**M**VGGVV
S3	DAEFRHDSGY EVHHQ**K**LVFF **A**EDV**G**S**N**KGA I**I**GLMVGGV**V**
S4	DAEFRHDSGY EVHHQK**LV**FF A**E**DVGSNKG**A** **I**I**G**LMVGGVV

Table S3. ^{13}C NMR chemical shifts for $RM_{CO520}A\beta_{40}$ and backbone dihedral angles predicted by TALOS-N.

	Chemical shift (ppm)[1]						
Residue	CO	C^{α}	C^{β}	C^{γ}	C^{δ}	C^{ε}	predicted ϕ, ψ (°)[2]
E11	172.0	52.9	31.1	33.5	180.2		
V12	173.1	57.8	31.2	19.7			-99 ± 13, 136 ± 11
K16	171.8	53.2	33.2	24.9	28.9	38.2	-123 ± 19, 150 ± 10
L17	172.3	52.2	44.7	24.5	nd[3]		-123 ± 13, 139 ± 8
V18	172.2	58.4	33.6	19.5			-123 ± 13, 133 ± 6
F19	171.8	54.0	41.2	136.1	129.0	nd	-122 ± 14, 147 ± 10
F20	169.7	54.3	41.2	135.7	129.2	nd	-138 ± 12, 154 ± 11
A21	172.6	48.4	21.5				-138 ± 11, 152 ± 10
E22	171.8	53.7	32.2	34.8	179.1		-141 ± 12, 149 ± 11
D23	173.0	*54*	*41*	*177*			-80 ± 13, 129 ± 20
V24							-97 ± 21, 131 ± 17
G25	170.5	42.9					78 ± 14, -162 ± 25
S26	172.6	54.6	62.7				-92 ± 26, 155 ± 14
N27	172.6	51.8	38.4	174.4			-90 ± 33, 137 ± 18
K28	173.4	53.6	32.6	25.5	27.8	40.3	-127 ± 31, 155 ± 20
G29							-149 ± 27, 172 ± 12
A30	172.6	49.6	21.0				-135 ± 13, 146 ± 9
I31	172.7	58.0	39.7	25.8, nd	12.3		-113 ± 15, 138 ± 10
I32	172.2	57.5	40.2	25.7, 16.1	12.5		-129 ± 9, 140 ± 11
G33	168.4	43.5					-162 ± 20, 179 ± 17
L34	171.6	51.8	44.5	24.7	nd		-133 ± 13, 142 ± 13
M35	171.6	52.8	34.1	30.9		nd	-121 ± 14, 132 ± 9
V36	172.2	58.2	32.2	18.9			-129 ± 13, 141 ± 12
G37							-148 ± 23, 163 ± 12
G38	168.8	43.1					
V39							-95 ± 10, 128 ± 7
V40	177.4	60.1	32.6	19.5			

[1] Chemical shifts referenced to neat TMS. The data with distribution larger than 1 ppm are italicized. [2] The data in red belonged to the class of "WARN", others were "STRONG". [3] nd: not determined.

Table S4: ^{13}C NMR chemical shifts for $RM_{CO520}A\beta_{42/40}$ and backbone dihedral angles predicted by TALOS-N.

	Chemical shift (ppm)						
Residue	CO	C^{α}	C^{β}	C^{γ}	C^{δ}	C^{ε}	predicted ϕ, ψ (°)
E11	173.0	52.8	29.9	35.0	180.3		
V12	172.2	58.9	31.4	19.2			-98 ± 20, 135 ± 10
K16	171.9	52.7	35.4	26.7	31.2	40.0	-128 ± 14, 148 ± 12
L17	172.6	52.0	44.0/41.5	24.7	nd		-121 ± 12, 134 ± 10
V18	171.8	58.8	32.7	19.9			-117 ± 15, 135 ± 6
F19	171.0	55.1	41.7	136.7	129.3	nd	-129 ± 14, 140 ± 12
F20	169.7	54.1	41.3	136.2	128.6	nd	-138 ± 13, 152 ± 13
A21	172.8	48.8	20.7				-135 ± 16, 146 ± 12
E22	173.7	52.3	30.0	35.0	180.6		
D23	nd	*51*	*40*	*178*			
V24							
G25	171.1	45.2					65 ± 8, -141 ± 13
S26	172.6	56.2	62.3				-101 ± 20, -4 ± 21
N27	172.4	51.2	38.0	173.8			-93 ± 13, 42 ± 65
K28	172.8	53.2	32.6	25.0	28.7	40.1	-141 ± 14, 153 ± 11
G29							-175 ± 36, -176 ± 26
A30	173.3	48.3	20.6				-135 ± 11, 151 ± 10
I31	172.6	58.3	40.1	26.1, nd	13.4		-119 ± 12, 131 ± 11
I32	172.2	57.8	nd	25.5, 15.9	12.0		-116 ± 16, 139 ± 10
G33	168.5	43.6					-166 ± 18, -180 ± 12
L34	171.7	51.7	45.2	24.9	nd		-132 ± 14, 144 ± 12
M35	171.5	52.3	34.2	31.6		nd	-122 ± 12, 134 ± 12
V36	172.3	58.2	32.1	19.0			-126 ± 14, 141 ± 13
G37							-149 ± 19, 165 ± 12
G38	169.3	42.3					
V39							-92 ± 13, 129 ± 7
V40	178.2	60.3	32.4	20.0			

Table S5. ^{13}C NMR chemical shifts for $RM_{CO520}A\beta_{42/40}$ fibrils and backbone dihedral angles predicted by TALOS-N.

	Chemical shift (ppm)						
Residue	CO	C^{α}	C^{β}	C^{γ}	C^{δ}	C^{ε}	predicted ϕ, ψ (°)
E11	173.7	53.6	31.8	nd	181.4		
V12	173.2	59.3	30.6	19.2			-87 ± 14, 135 ± 8
K16	171.4	53.2	33.8	23.6	27.9	40.4	-126 ± 14, 148 ± 12
L17	172.6	52.2	43.6	25.4	nd		-115 ± 14, 136 ± 10
V18	172.7	58.8	33.2	19.4			-122 ± 12, 137 ± 7
F19	170.3	54.5	41.7	136.3	128.5	nd	-135 ± 12, 150 ± 13
F20	170.9	54.7	41.9	136.0	127.7	nd	-137 ± 12, 150 ± 13
A21	172.9	47.9	21.2				-137 ± 12, 153 ± 10
E22	173.6	52.0	33.3	35.1	181.1		-136 ± 10, 147 ± 12
D23	173.3	53.5	39.9	177.6			-72 ± 8, 139 ± 13
V24							-109 ± 16, 120 ± 43
G25	171.0	45.2					86 ± 10, -170 ± 12
S26	172.4	55.1	63.4				-106 ± 34, 142 ± 17
N27	172.1	51.2	39.1	173.8			-106 ± 24, 133 ± 11
K28	173.2	53.4	32.1	nd	27.4	39.9	-123 ± 33, 151 ± 20
G29							-124 ± 41, -178 ± 20
A30	173.2	48.1	20.2				-128 ± 14, 145 ± 13
I31	172.5	58.4	40.4	26.0, 15.3	13.1		-120 ± 13, 138 ± 11
I32	172.1/173.8	55.8/58.0	40.3	24.9, 15.2	12.2		-129 ± 9, 146 ± 10
G33	168.4	43.5					-165 ± 17, 179 ± 15
L34	171.6	51.5	44.6	24.7	nd		-132 ± 12, 144 ± 11
M35	172.2	52.7	35.1	32.1		nd	-119 ± 11, 133 ± 8
V36	173.0	57.4	32.7	19.3			-126 ± 14, 142 ± 13
G37							-152 ± 15, 166 ± 10
G38	168.6	43.1					
V39							-96 ± 10, 131 ± 9
V40	178.4	59.3	32.7	19.8			

REFERENCES

(1) Efron, B. Bootstrap Methods: Another Look at the Jackknife. *Ann. Stat.* **1979**, *7* (1), 1–26.

(2) Jones, E.; Oliphant, T.; Peterson, P. SciPy: Open Source Scientific Tools for Python. http://www.scipy.org

(3) Nocedal, J.; Wright, S. J. *Numerical Optimization*, 2nd ed. Springer Series in Operations Research and Financial Engineering. Springer: New York, **2006**.

(4) Cohen, S. I. A.; Linse, S.; Luheshi, L. M.; Hellstrand, E.; White, D. A.; Rajah, L.; Otzen, D. E.; Vendruscolo, M.; Dobson, C. M.; Knowles, T. P. J. Proliferation of Amyloid-B42 Aggregates Occurs through a Secondary Nucleation Mechanism. *Proc. Natl. Acad. Sci.* **2013**, *110*, 9758–9763.

(5) Takegoshi, K.; Nakamura, S.; Terao, T. C-13-H-1 Dipolar-Assisted Rotational Resonance in Magic-Angle Spinning NMR. *Chem Phys Lett*. **2001**, *344*, 631–637.

(6) Morcombe, C. R.; Gaponenko, V.; Byrd, R. A.; Zilm, K. W. Diluting Abundant Spins by Isotope Edited Radio Frequency Field Assisted Diffusion. *J. Am. Chem. Soc.* **2004**, *126*, 7196–7197.

(7) Bennett, A. E.; Rienstra, C. M.; Auger, M.; Lakshmi, K. V.; Griffin, R. G. Heteronuclear Decoupling in Rotating Solids. *J. Chem. Phys.* **1995**, *103*, 6951–6958.

(8) Harris, R. K.; Becker, E. D.; De Menezes, S. M. C.; Granger, P.; Hoffman, R. E.; Zilm, K. W. Further Conventions for NMR Shielding and Chemical Shifts IUPAC Recommendations 2008 (Reprinted from Pure Appl Chem, Vol 80, Pg 59, 2008). *Solid State Nucl. Magn. Reson.* **2008**, *33*, 41–56.

(9) Hu, X.; Crick, S. L.; Bu, G.; Frieden, C.; Pappu, R. V.; Lee, J.-M. Amyloid Seeds Formed by Cellular Uptake, Concentration, and Aggregation of the Amyloid-Beta Peptide. *Proc. Natl. Acad. Sci.* **2009**, *106* (48), 20324–20329.

(10) Ruan, Z.; Pathak, D.; Venkatesan Kalavai, S.; Yoshii-Kitahara, A.; Muraoka, S.; Bhatt, N.; Takamatsu-Yukawa, K.; Hu, J.; Wang, Y.; Hersh, S.; Ericsson, M.; Gorantla, S.; Gendelman, H. E.; Kayed, R.; Ikezu, S.; Luebke, J. I.; Ikezu, T. Alzheimer's Disease Brain-Derived Extracellular Vesicles Spread Tau Pathology in Interneurons. *Brain J. Neurol.* **2020**.

(11) Yang, C.-I.; Tsai, B. N. F.; Huang, S.-J.; Wang, T.-Y.; Tai, H.-C.; Chan, J. C. C. Aggregation of Beta-Amyloid Peptides Proximal to Zwitterionic Lipid Bilayers. *Chem. Asian J.* **2015**, *10* (9), 1967–1971.

(12) Guo Zhong-Hong; Yang Chien-I; Ho Cheng-I; Huang Shing-Jong; Chen Yin-Chung; Tai Hwan-Ching; Chan Jerry Chun Chung. Fibrillization of B-Amyloid Peptides via Chemically Modulated Pathway. *Chem. – Eur. J.* **2018**, *24* (19), 4939–4943.

(13) Rajput, S.; Sani, M.-A.; Keizer, D. W.; Separovic, F. Utilizing Magnetic Resonance Techniques to Study Membrane Interactions of Amyloid Peptides. *Biochem. Soc. Trans.* **2021**, *49* (3), 1457–1465.

(14) Lin, Y.-L.; Cheng, Y.-S.; Ho, C.-I.; Guo, Z.-H.; Huang, S.-J.; Org, M.-L.; Oss, A.; Samoson, A.; Chan, J. C. C. Preparation of Fibril Nuclei of Beta-Amyloid Peptides in Reverse Micelles. *Chem. Commun.* **2018**, *54* (74), 10459–10462.

(15) Yeung, P. S.-W.; Axelsen, P. H. The Crowded Environment of a Reverse Micelle Induces the Formation of β-Strand Seed Structures for Nucleating Amyloid Fibril Formation. *J. Am. Chem. Soc.* **2012**, *134* (14), 6061–6063.

(16) Yeung, P. S.-W.; Eskici, G.; Axelsen, P. H. Infrared Spectroscopy of Proteins in Reverse Micelles. *Biochim. Biophys. Acta BBA - Biomembr.* **2013**, *1828* (10), 2314–2318.